Cloud phase and macrophysical properties over the Southern Ocean during the MARCUS field campaign

Baike Xi[1], Xiquan Dong[1], Xiaojian Zheng[1], and Peng Wu[2]

[1]Department of Hydrology and Atmospheric Sciences, University of Arizona, Tucson, AZ, USA

[2]Pacific Northwest National Laboratory, Richland, WA, USA

Correspondence: Baike Xi (baikex@arizona.edu)

Abstract.

To investigate the cloud phase and macrophysical properties over the Southern Ocean (SO), the Department of Energy (DOE) Atmospheric Radiation Measurement (ARM) Mobile Facility (AMF2) was installed on the Australian icebreaker *Aurora Australis* during the MARCUS field campaign [41 to 69 ºS; 60 to 160 ºE] from October 2017 to March 2018. To examine cloud properties over the mid-latitude and Polar regions, the study domain is separated into northern (NSO) and southern (SSO) parts of the SO with a demarcation line of 60 °S. The total cloud fractions (*CF*s) were 77.9 %, 67.6 %, and 90.3 % for the entire domain, NSO and SSO, respectively, indicating that higher *CF*s were observed in the Polar region. Low-level clouds and deep convective clouds are the two most common cloud types over the SO.

A new method was developed to classify liquid, mixed-phase and ice clouds in single-layered low-level clouds (LOW) where mixed-phase clouds dominate with an occurrence frequency (*Freq*) of 54.5 %, while the *Freq* of the liquid and ice clouds were 10.1 % (most drizzling) and 17.4 % (least drizzling). The meridional distributions of low-level cloud boundaries are nearly independent of latitude, whereas the cloud temperatures increased ~8 K and atmospheric precipitable water vapor increased from ~5 mm at 69 °S to ~18 mm at 43 °S. The mean cloud liquid water paths over NSO were much larger than those over SSO. Most liquid clouds occurred over NSO with very few over SSO, whereas more mixed-phase clouds occurred over SSO than over NSO. There were no significant differences for ice cloud *Freq* between NSO and SSO. The ice particle sizes are comparable to cloud droplets and drizzle drops, and well mixed in the cloud layer. These results will be valuable for advancing our understanding of the meridional and vertical distributions of clouds and can be used to improve model simulations over the SO.

1. Introduction

The Southern Ocean (SO) is one of the cloudiest and stormiest regions on the Earth (Mace et al., 2009; Chubb et al., 2013). Over the SO, most of the aerosols are naturally produced via oceanic sources given the remote environment. The uncertainties of aerosol forcing caused by natural emissions have larger variances than anthropogenic emissions, especially the dimethyl sulfide (DMS) flux contributes significantly to the bias (Carslaw et al., 2013). The SO is a unique natural laboratory to address the natural aerosol emissions and their contributions to the biases because it has rich ecosystems and is remote to human activities (McCoy et al., 2015). However, we have limited knowledge about cloud formation processes within such clean environments and their associated aerosol and cloud properties. The unique nature of the SO region features low-level supercooled liquid and mixed-phase clouds, which is significantly different from the subtropical marine boundary layer (MBL) clouds where warm liquid clouds are dominant (Dong et al., 2014; Wu et al., 2020; Zhao et al., 2020), and also different to the Arctic mixed-phase clouds which are featured with the liquid-topped cloud layer with ice cloud layer beneath (Qiu et al., 2015).

Large biases in cloud amount and microphysics over the SO in the Coupled Model Intercomparison Project phase 5 (CMIP5) climate models result in a near 30 W m^{-2} shortwave radiation deficit at the top of the atmosphere (TOA) (Marchand et al., 2014; Stanfield et al., 2014, 2015), which further leads to unrealistic cloud feedbacks and equilibrium climate sensitivity (Bony et al., 2015; Stocker et al., 2013). Meanwhile, the efficiency of aerosol-cloud interaction (ACI) over the SO was found to be crucial for the models' sensitivities to the radiation budget. A new aerosol scheme in the Hadley Centre Global Environmental model can dampen the ACI and suppress negative clear-sky shortwave feedback, both of which contribute to a larger climate sensitivity (Bodas-Salcedo et a., 2019).

A climate sensitivity study using CMIP6 general circulation models (GCMs) shows much higher temperature variations across 27 GCMs in response to doubled CO_2 than those in CMIP5, which may have resulted from the decreased extratropical low-level cloud cover and cloud albedo over the SO in CMIP6 (Zelinka et al., 2020). Low-level clouds are a key climate uncertainty and can explain 50 % of the inter-model variations (Klein et al., 2017) because conversion from liquid cloud droplets to ice cloud particles decreases the cloud albedo and reduces the reflected shortwave radiation at TOA. Models, however, have difficulties accurately partitioning the cloud phase (Kalesse et al., 2016). The phase changes in mixed-phase clouds over the Arctic have proved to affect the cloud lifetime and radiative properties significantly, that is, converting from ice cloud particles to liquid cloud droplets may increase the cloud optical depth and the reflected shortwave radiation at TOA (Morrison et al., 2012). In contrast, models that allow mixed-phase clouds to glaciate rapidly can produce 30% more warming from doubling CO_2 (McCoy et al., 2014).

Phase transition processes have been investigated by several groups using both satellite and ground-based measurements. For instance, Mace and Protat (2018) found that there are more mixed-phase clouds over the SO measured from the ship than retrieved from CloudSat and CALIPSO measurements because the satellites cannot accurately measure clouds below ~1 km. Lang et al. (2018) used a model to investigate the clouds under post cold frontal systems and found large biases in model simulations and concluded that the cloud cover and radiative biases over the SO are highly regime dependent. Of all cloud types, low-level clouds are primarily responsible for the biases in the model simulations due to the lack of reliable measurements, which leads to a poor understanding of the conditions where these clouds form and the phase(s) that result. In other words, a physical representation of clouds, especially for low-level clouds, is unclear but truly necessary for improving model simulations. Therefore, reliable observations of the cloud macro-

93   and micro-physical properties from ground-based active and passive remote sensors are crucial for

94   the improvement of model simulations.

95   Previous studies show that cloud phase is primarily dependent on cloud temperature, and the

96   transition from one cloud phase to another will modify the cloud optical properties, which further

97   affects the radiation budgets (Hu et al., 2010; Intrieri et al., 2002; Morrison et al., 2012). Based on

98   satellite observations and retrievals, Hu et al. (2010) found that supercooled liquid water (SLW)

99   clouds are most common in the low-level clouds over the SO, where 80% of low-level clouds

100   contain SLW in a wide range of cloud temperatures from 0°C to −40°C. The formation of SLW

101   clouds is usually related to strong boundary layer convection. However, when ice nuclei exist in

102   the mixed-phase clouds, the ice particles can grow quickly and become bigger through consuming

103   supercooled liquid water drops. The SLW is inherently unstable due to the higher vapor pressure

104   over liquid than over ice and the quicker vapor deposition on ice particles than on liquid droplets

105   (Intrieri et al., 2002). As the supercooled liquid cloud droplets glaciate to ice particles, the cloud

106   layer becomes darker because the ice particles scatter less shortwave radiation and absorb more

107   radiation in the near IR wavelength regime. It is unclear, however, what role these ice particles

108   play in the low-level clouds over the SO, which includes the impact on drizzle development.

109   During HIAPER Pole-to-Pole Observation (HIPPO) campaigns, Chubb et al. (2013) found that

110   there are rarely ice particles in non-drizzling and light drizzling clouds over the SO, which may

111   imply that the ice particles in the mixed-phase clouds may modulate the drizzle formation.

112   To investigate the aerosol and cloud properties over the SO, a field campaign called the

113   Measurements of Aerosols, Radiation, and Clouds over the Southern Ocean (MARCUS) was

114   conducted using the ship-based measurements between Hobart, Australia, and the Antarctic during

115   the period October 2017-March 2018. The Department of Energy (DOE) Atmospheric Radiation

116 Measurement (ARM) Mobile Facility (AMF2) was installed on the Australian icebreaker *Aurora*

117 *Australis,* which voyaged from Hobart, Tasmania to the Australian Antarctic stations of Casey,

118 Mawson, and Davis, as well as Macquarie Island as illustrated in Fig. 1. Another field campaign,

119 called South Ocean Clouds, Radiation, Aerosol Transport Experimental Study (SOCRATES) field

120 campaign was conducted during austral summer from January 15 to February 26, 2018. In this

121 study, the aircraft in-situ measurements during SOCRATES are used as the reference for the

122 analysis. The SOCRATES domain is shown in the black dotted rectangle box in Fig. 1. The

123 objectives of the MARCUS campaign are to investigate the vertical distribution of boundary layer

124 clouds and reveal the reasons why the mixed-phase clouds are common in the warm season

125 (McFarquhar et al., 2016; McFarquhar et al., 2021). Our study will focus on cloud macrophysical

126 properties and cloud phase along the shiptracks during MARCUS.

127 MARCUS ship-based instruments include AMF2 cloud radar, lidar, microwave radiometer,

128 micropulse lidar, radiosonde sounding, precision solar pyranometer and precision infrared

129 radiometer, as well as aerosol sensors. Through these comprehensive observations over the SO,

130 we are tentatively answering the following three scientific questions:

131 (1) What is the total cloud fraction over the SO during MARCUS, as well as vertical and

132 meridional variations in cloud fraction?

133 (2) What are the dominant cloud types over the SO, their associated cloud phase and

134 macrophysical properties, as well as their vertical and meridional distributions?

135 (3) What are the vertical and meridional distributions of the low-level clouds over the SO?

136 This manuscript is organized as follows: the data and method and introduced in section 2. The

137 statistical results for all clouds during MARCUS are summarized in section 3. The low-level cloud

138   phase and macrophysical properties are described in section 4, followed by a summary and

139   conclusions in section 5.

2. Data and Method

2.1 Ship-based measurements used in this study

142   The AMF2 instruments, measurements, and their corresponding uncertainties and references

143   are listed in Table 1. Because AMF2 was designed to support shipboard deployments, the baseline

144   suite of instruments are marine-focused, including the 95-GHz W-band cloud radar (WACR),

145   ceilometer, micropulse lidar (MPL), microwave radiometer (MWR), aerosol observation system

146   (AOS), meteorological measurements (MET, includes the following data: temperature, pressure,

147   specific humidity, wind direction and speed) on the ship, rain gauge and the radiosonde soundings.

148   The combined cloud radar and ceilometer measurements can provide the cloud boundaries as long

149   as there are no optically thin clouds and the cloud-base heights (H_{base}) are not greater than the

150   upper limit (7.7 km) of the ceilometer. The micropulse lidar will be used to identify optically thin

151   clouds and the clouds with $H_{base} > 7.7$ km. A previous study has shown that these additional clouds

152   detected by the micropulse lidar can be a non-negligible supplement to the total cloud fraction

153   (Mace et al., 2021). A detailed description of the instruments and the cloud parameters during

154   MARCUS can be found in Mace et al. (2021) and McFarquhar et al. (2016 and 2021).

155   The cloud occurrence frequency can be determined through two steps: the column cloud

156   fraction is simply the ratio of cloudy samples to the total observations in every 5-min; the

157   occurrence frequency for each type of cloud during the entire time period equals the ratio of the

158   number where column cloud fraction is greater than zero to the total 5-min samples. In order to

159   accurately estimate the cloud temperatures, we adopted a linear interpolation method based on the

160   daily balloon soundings (4 to 5 times per day) to achieve a better temporal resolution of the vertical

161 profiles of temperature, pressure, and specific humidity. The method considers MET

162 measurements to ensure vertical continuity and adjacent soundings for temporal continuity. Using

163 these interpolated atmospheric profiles, cloud temperatures can be obtained at a 5-min temporal

164 resolution.

165   The cloud liquid water path (*LWP*) and atmospheric precipitable water vapor (*PWV*) are

166 retrieved based on a physical-iterative algorithm using observations of the microwave radiometer

167 brightness temperatures at 23.8 and 31.4 GHz with uncertainties ranging from 15 to 30 g m^{-2}

168 (Marchand et al., 2003). It is important to note that the brightness temperature biases switch signs

169 among different climatological regions because a threshold of 5 ℃ in cloud-base temperature was

170 used in their physical retrievals. Since the retrieved LWP and PWV are based on the MWR

171 measured brightness temperatures at two frequencies, any biases on the brightness temperatures

172 will affect these retrievals. Therefore, we propose an extra step to determine the uncertainties

173 during MARCUS. Based on the temperature profiles, we can identify clouds that are not likely to

174 contain liquid (e.g., pure ice-cloud), then we can estimate the LWP uncertainty based on their

175 corresponding retrieved LWP values. From the probability density function (PDF_ analysis, the

176 LWP uncertainty is estimated as 10 g m^{-2} for MARCUS.

177   To determine the precipitation status, the AOS and rain gauge measurements were used to

178 determine whether rain is reaching the surface qualitatively, but not quantitatively in this study.

179 All the measurements were averaged over 5 minutes, except the radar reflectivity, Doppler velocity,

180 and spectrum width used in Section 4.3.

181   **2.2 Cloud type classification and single-layer low cloud phases**

182   A classification method developed in Xi et al. (2010) was used to categorize different types of

183 clouds using ARM radar-lidar estimated cloud base (H_{base}) and top (H_{top}) heights and cloud

184   thickness (ΔH). A brief description of the classification of cloud types is as follows (Table 1 and

185   Figure 6 in Xi et al., 2010). The single-layered low-level clouds (LOW) is the fraction of time

186   when low clouds with $H_{top} \leq 3$ km occur without clouds above them. Middle clouds (MID) range

187   from 3 to 6 km without any clouds below and above, while high clouds (HGH) have $H_{base} > 6$ km

188   with no cloud underneath. Other types of clouds are defined by different combinations of the above

189   three types, middle over low (MOL), high over low (HOL), high over middle (HOM), and the

190   cloud column through the entire troposphere is defined as HML. Three types, MOL, HOM, and

191   HML, include both contiguous and non-contiguous cloud layers, and their thicknesses may be

192   overestimated when clear layer(s) are present between any two cloud layers.

193   Furthermore, we used the measurements of interpolated sounding, microwave radiometer

194   retrieved *LWP*, radar reflectivity, Doppler velocity and spectrum width to classify the cloud phase

195   in each radar range volume of low-level clouds during MARCUS. The detailed classification

196   method will be introduced in Section 4.1. We also used ERA-Interim reanalysis data to study the

197   environmental conditions during MARCUS. The lower tropospheric stability (LTS) is calculated

198   from the potential temperature difference between the surface and 700 hPa to assess the boundary-

199   layer stabilities when the low-level clouds appeared along the shiptracks. The relative

200   contributions of mixed-phase, liquid and ice clouds to the single-layered low-level clouds as well

201   as their drizzling status are also analyzed in this study. The latitudinal and longitudinal variations

202   of the single-layered low-level clouds as well as their vertical distributions are further explored in

203   this study.

204   **3. Statistical results for all clouds during MARCUS**

205   The occurrence frequencies of total cloud cover and different types of clouds and their

206   associated properties over the entire study domain during MARCUS are presented in Figs. 2 - 4.

207 In order to examine the cloud properties over the mid-latitude and Polar regions, we separate the

208 SO domain into northern (NSO, north of 60°S) and southern (SSO, south of 60°S) parts using a

209 demarcation line of 60ºS. A total of 2,447 hours cloud samples were collected during MARCUS

210 in this study, in which 1,181 hours of samples were located in the NSO and 1,266 hours of samples

211 were collected from the SSO. It is important to note that adding micropulse lidar measurements

212 increased the total samples of non-liquid-containing clouds by ~20% because micropulse lidar is

213 more sensitive to optically thin clouds than cloud radar. However, micropulse lidar signals are

214 usually attenuated and cannot provide a meaningful signal when the liquid cloud layer is thicker

215 than a couple of hundred meters (Sassen, 1991).

216 Figure 2 shows the vertical distributions of total cloud cover over the entire domain, as well as

217 over NSO and SSO. For the vertical distributions, the occurrence frequencies of total cloud

218 increase from the first radar gate (~ 226 m) to ~700 m, then monotonically decrease with altitude

219 with a few small increments at different levels, especially over SSO. Comparing the occurrence

220 frequencies of total cloud between NSO and SSO, we can draw the following conclusions. 1) The

221 SSO has more cloudiness than the NSO under 7 km, while the NSO has more cloudiness than the

222 SSO above 7 km. 2) Below 3 km, the occurrence frequencies of clouds over the NSO decrease

223 dramatically from 37 % at an altitude of ~700 m to 16 % at 3 km and from 45 % to 28 % over the

224 SSO, which is similar to the vertical distributions of the low-level clouds over some Northern

225 Hemisphere mid-latitude regions, such as Eastern North Atlantic (ENA, Dong et al., 2014). The

226 occurrence frequencies measured during MARCUS are much lower than these shown in Fig. 8 of

227 Mace et al., (2009) throughout the entire vertical column between the same range of latitudes,

228 especially, the occurrence frequencies during MARCUS are almost half of those measured by

229 CloudSat and CALIPSO from 1 to 3 km. The reason has been explained in Xi et al., (2010), that

230 is, a comparison of occurrence frequencies between measurements of two different platforms can

231 only be performed under an equivalent spatial-to-temporal resolution. In other words, our results

232 were calculated under 5-min temporal resolution, and the results in Mace et al., (2009) were

233 statistically in the 2º gridbox. Therefore, the comparison between these two results is not

234 reasonable. To make a fair comparison, one has to know the cloud amount at each area or time

235 step, then the product of amount and frequency is independent of either temporal and spatial

236 measurement.

237   To compare with other studies, we calculated the cloud fractions (CFs) of total and different

238 types of clouds. The total CFs were 77.9 %, 67.6 %, and 90.3 % for the entire domain, NSO and

239 SSO, respectively, indicating that 22.7 % more clouds occurred in the Polar region than in the mid-

240 latitude region. The total CF over the entire domain is very close to the 76 % calculated by Mace

241 and Protat (2018) using ship-based measurements during the Cloud, Aerosols, Precipitation,

242 Radiation and Atmospheric Composition (CAPRICORN) field experiment. The total CF over the

243 SSO is close to that estimated by using the complementarity of CALIOP lidar aboard CALIPSO

244 and CPR aboard CloudSat (DARDAR version 2 data) from Listowski et al. (2019).

245   Figiure 3 shows the occurrence frequencies of categorized clouds and their cloud boundaries

246 using the maximum H_{top} and the minimum H_{base} if there are two or more layers in each 5-min

247 sample. For example, the mean H_{base} and H_{top} for single-layered low-level (LOW) are 0.92 km and

248 1.62 km, respectively, listed in Table 2, which are the average values of min H_{base} and max H_{top} in

249 LOW category. As illustrated in Fig. 3a, the single-layered low-level (LOW), deep cumulus or

250 multi-layered (HML), and MOL clouds are the three dominant types of clouds over the SO.

251 Comparing the clouds between NSO and SSO, all types of clouds in SSO have higher frequency

252 of occurrence than those in NSO except HOL. The differences range from less than 1 % (LOW)

253 to more than 10 % (MOL). Comparing the clouds over mid-latitude oceans between the two

254 hemispheres, i.e., between NSO and ARM ENA site (Dong et al., 2014), we find: (1) The total

255 cloud fractions (CFs) are close to each other (67.6 % over NSO vs. 70.1 % at ARM ENA); (2)

256 LOW CFs are 22.9 % vs. 27.1 %, which is the dominant type of cloud in both regions; and (3)

257 Both MOL and HML clouds, including underneath low clouds, are 14.2 % and 16.5 % over NSO,

258 much higher than those (4.2 % and 12.1 %) at ARM ENA site, indicating that there are more MOL

259 and deep convective clouds over NSO than over ENA.

260   Figure 3b shows the vertical locations of different types of cloud layers, which represent the

261 mean H_{top} and H_{base} listed in Table 2 for any type of cloud. Nearly all H_{top} and cloud thickness (ΔH)

262 values over NSO are higher or deeper than those over SSO, presumably due to stronger solar

263 radiation and stronger convection over NSO. H_{base} values basically followed their cloud-top

264 counterparts with a couple of exceptions. These cloud macrophysical properties are closely

265 associated with large-scale dynamic patterns and environmental conditions. By analyzing the

266 ERA-Interim reanalysis (not shown), the 850 hPa geopotential heights show persistent westerlies

267 with slightly higher geopotential heights over the northwest corner of the domain, which may

268 closely relate to the higher H_{top} over NSO than over SSO. Furthermore, the boundary layer over

269 NSO is relatively more stable than over SSO based on lower troposphere stability (LTS) analysis

270 (12.2-15.32 K over NSO vs. 11.48-13.29 K over SSO).

271   When we plot the probability density functions (PDFs) of cloud LWPs for different types of

272 clouds, we find that the PDFs of LWPs for HGH and HOM peak are less than 10 g m^{-2}. These

273 results make physical sense because HGH clouds should not contain any liquid droplets, and most

274 HOM clouds, especially those over SSO, should be ice phase dominant. In addition, the 10 g m^{-2}

275 of LWP is close to the uncertainty of the LWP retrieval in Marchand et al., (2003). Therefore, this

276 value is used as a threshold for all types of clouds, which leads to less than one percent reduction

277 of the total samples. As shown in Fig. 4a, the LWPs (> 10 g m^{-2}) for all types of clouds are much

278 higher over NSO than over SSO because the low-level and MOL clouds in the mid-latitudes

279 contain more liquid water than those in Polar regions. The mean LWPs for liquid containing low-

280 level and middle-level clouds over NSO, i.e. LOW, MID and HOL, range from ~130 to 150 g m^{-}

281 ^{2}, while the mean LWPs for MOL and HML are two times higher (~270 g m^{-2}) than the mean LWP

282 of LOW, MID and HOL. Note that the mean LWPs for most types of clouds over the SSO are

283 much lower than those over the NSO, except for the LOW clouds.

284   The occurrence frequencies of LWPs (> 10 g m^{-2}) over NSO and SSO contradict their cloud

285 LWP values as demonstrated in Fig. 4b. To further investigate the amount of available precipitable

286 water vapor (PWV), we found that mean PWV values in SSO are at least 2 to 3 times less than

287 those in NSO for same types of clouds (figure not shown). Note that the samples of MID, HGH,

288 and HOM clouds are excluded from this study when they have LWPs less than 10 g m^{-2}, since

289 these low LWPs are within the retrieval uncertainty of cloud LWP and hence may not contain any

290 liquid cloud droplets. The higher LWPs, larger cloud droplets, drizzle drops and ice particles, and

291 greater drizzling occurrence frequencies over NSO (which is discussed later) will lead to the quick

292 dissipation of clouds over NSO. In contrast to NSO, the SSO cloud LWPs and particle sizes are

293 much smaller with less drizzling events, which increases cloud lifetime relative to NSO. The 67.6 %

294 and 90.3 % CFs over NSO and SSO provide strong evidence for this argument. We can draw the

295 following conclusions by comparing the cloud macrophysical properties between NSO and SSO

296 in Figs. 3 and 4. The LOW fraction, thickness, and LWP over NSO and SSO are comparable to

297 each other. For other types of clouds, cloud thicknesses are similar to each other or slightly deeper

298 over NSO, but the cloud LWPs over NSO are much larger than those over SSO, resulting in more

299   precipitation events over NSO. As pointed out in Albrecht (1989), more precipitation events may

300   reduce the cloud lifetime. This argument is consistent with the results shown in Figs. 2 and 3a for

301   all clouds except for HOL. Cloud lifetimes over NSO are shorter than those over SSO, which leads

302   to lower *CF*s over NSO than over SSO.

303   Table 2 provides a summary of the mean, standard derivation, minimum and maximum for

304   cloud boundaries, LWP and the percentage of multi-layered cloud for each cloud type over the SO.

305   Non-contiguous (multi-layer) clouds over the SO occur very frequently, especially for HOM and

306   HML. The *LWP* for single-layered clouds is greater than that for multi-layered clouds. The *LWP*

307   for single-layered HML almost doubles that for multi-layered HML.

308   **4.   Single-layered low-level clouds**

309   As discussed in Section 3, single-layered low-level clouds (LOW) are the dominant cloud type

310   in both northern (NSO) and southern (SSO) parts of the SO. Figs. 3 and 4 further reveal that LOW

311   cloud type is the only one having comparable *CF*, cloud, thickness, *LWP* over both NSO and SSO.

312   This warrants further study: Are the cloud phases, properties, and vertical and meridional

313   variations of LOW clouds over these two regions similar to each other or significantly different?

314   **4.1. Cloud phase**

315   In this study, cloud boundaries are determined by combining cloud radar, ceilometer and

316   micropulse lidar measurements at a temporal resolution of 5-min. The cloud phase, liquid water

317   droplets or ice particles, are determined in each radar range volume. A flow chart for classifying

318   the phases of single-layered low-level clouds is drawn in Fig. 5. The determination of warm liquid

319   clouds is straightforward using both cloud-base (T_{base}) and -top (T_{top}) temperatures greater than 0

320   °C, and cloud *LWP*s greater than the threshold (10 g m^{-2}). The determination of supercooled liquid

321   clouds is slightly complicated. When either T_{base} or T_{top} is below 0° C, and cloud *LWP*s are greater

322 than the threshold, the radar Doppler spectrum width (WID) and velocity (V_d) are used for the

323 determination of supercooled liquid water clouds. If the majority (10 seconds of original radar

324 measurements) of WID within a 5-min period are less than 0.4 m s^{-1} and V_d are equal to or less than

325 0.0 m s^{-1} (updrafts) in the volume, then this range volume is defined as supercooled liquid clouds.

326   Mixed-phase clouds are determined when the median (calculated from 10 seconds of original

327 radar measurements) of WID is greater than 0.4 m s^{-1} or V_d is greater than 0.0 m s^{-1} (downdrafts)

328 due to the existence of large ice particles in the clouds. If cloud LWP is below the threshold, then

329 it is defined as an ice cloud, otherwise it is defined as a mixed-phase cloud. It is worth mentioning

330 that large ice particles, which grow through vapor deposition or rime processes, dominate the radar

331 reflectivity and are heavier than cloud droplets. Therefore, these large ice particles not only

332 broaden the spectrum width but also have relatively large fall speeds.

333   To further evaluate our classification method, we compared the classified mixed-phase and ice

334 clouds with the micropulse lidar linear depolarization ratios (LDR) as an extra measure. The LDR

335 ranges follow the method in Shupe et al., (2005), which are $0.11 < LDR < 0.15$ for mixed-phase

336 clouds, and $LDR > 0.15$ for ice clouds as listed in Table 1. Table 3a shows the quantitative

337 comparison of the cloud phase identifications between these two classification methods. The

338 numbers represent the counts of each matched 5-min sample, where the diagonal numbers indicate

339 that both methods are identifying the same type of cloud phase. In general, the two methods have

340 89 % agreement on the phase identification. Secondly, we performed the phase classification

341 directly from microphysical probes onboard G-1 aircraft during SOCRATES and treated them as

342 'ground-truth' (Mohrmann et al., 2021). Since the in-situ cloud microphysical measurements can

343 tell us the phase of the cloud, it allows us to see the percentage variations of cloud phase, by

344 changing integration time of in-situ sampling to mimic what the radar may observe the cloud for

345   each range volume. Table 3b shows possible cloud phase partitionings that may be detected by

346   cloud radar. As sampling time increases from 1 second to 30 seconds, more mixed-phase clouds

347   and fewer single-phase clouds can be observed.

348   Figure 6 shows the determination of mixed-phase and ice clouds through combined

349   measurements of radar reflectivity and spectrum width, lidar LDR and backscatter, and cloud LWP.

350   For the classified ice clouds, cloud LWPs are lower than 10 gm^{-2} (Fig. 6f), most of the Doppler

351   spectrum widths range from 0.08 to 0.16 m s^{-1} (Fig. 6b) and the *LDR* ratios (Fig. 6d) can be greater

352   than ~0.15, representing a narrow range of ice particle size distribution with higher *LDR* ratios.

353   For the classified mixed-phase clouds, cloud LWPs are greater than 10 gm^{-2} and most of the

354   Doppler spectrum widths range from 0.15 to 0.5 m s^{-1}, representing a broad particle size

355   distribution resulting from the mixture of liquid droplets and ice particles. An interesting result

356   occurs where both *LDR* signals (>0.2) and LWPs are much higher during the drizzling periods

357   (Fig. 6a), indicating a mixed-phase cloud with cloud droplets within the cloud layer and large

358   liquid drizzle drops and ice crystals below cloud base.

359   Based on the Doppler velocity, the mode values for both mixed-phase and ice clouds occur at

360   ~ 0.5 m s^{-1}, where the ice particles are dominant in both types of clouds. The broader particle size

361   distribution with lower *LDR* ratios for mixed-phase clouds and narrower particle size distribution

362   with higher *LDR* ratios for ice clouds further corroborate that the classified results from this study

363   are consistent with the traditional micropulse lidar *LDR* method.

364   It is important to note that the micropulse lidar signals are usually attenuated and cannot

365   provide a meaningful signal when the liquid cloud layer is thicker than a couple of hundred meters

366   (Sassen, 1991). Arctic mixed-phase clouds are typical with the liquid-dominant layer on the top of

367   the mixed-phase clouds and the ice-dominant layer underneath. The ceilometer-derived cloud-base

368 height represents the base of the liquid-dominant layer near the cloud top, while MPL-derived

369 cloud-base height represents the base of the lower ice-dominant layer (Qiu et al., 2015; Shupe,

370 2007; Shupe et al., 2005). Over the Arctic, the micropulse lidar signals can penetrate through the

371 ice-dominant layer to the liquid-dominant layer. However, the mixed-phase clouds over the

372 Southern Ocean are totally different from those over the Arctic region: they are well mixed (liquid

373 droplets and ice particles) from cloud base to cloud top, which is found in this study. Thus, the

374 micropulse lidar signals can be attenuated in the mixed-phase clouds over the Southern Ocean.

375 Statistical results show that 43 % of micropulse lidar signals were attenuated during MARCUS

376 compared to our classified results.

377 This classification method is further supported by the onboard cloud radar measurements

378 during the Southern Ocean Clouds Radiation Aerosol Transport Experimental Study (SOCRATES,

379 not shown). In that campaign, the reflectivity measurements were usually greater, and the spectrum

380 widths were much wider when the aircraft observed large ice particles compared to the time

381 periods when liquid cloud droplets were observed. Although the wider spectrum widths might be

382 caused by Doppler broadening of the moving aircraft, further analysis shows that the onboard radar

383 sends the signals (assuming the time of transmitted and received signals is short enough comparing

384 to aircraft speed) in the perpendicular to the movement of the aircraft, that is, there is no relative

385 movement between radar signals and clouds. Thus, the onboard radar spectrum width

386 measurements should be not significantly impacted by Doppler broadening (relative movement in

387 the same direction).

388 In this study, a total of 6,934 5-min single-layered low-level cloud samples were determined

389 using our classificaiton method, including 697 liquid cloud samples, 3,777 mixed, 1,205 ice, and

390 1,255 'OTHER' clouds. The category of 'OTHER' clouds represents more than one phase in each

391   column. Note that though the 'OTHER' is also mixed-phase cloud, it has different vertical

392   distribution of liquid compared to the 'mixed' cloud. It is also worth mentioning that about 5.5 %

393   of single-layered low-level cloud phases cannot be determined when the radar measurements were

394   not available during MARCUS, those were not accounted to "OTHER".

395   Figure 7 (upper panel) shows the drizzling status for each categorized cloud type, i.e., no rain

396   (yellow-green), virga (brown) and rain (navy blue). The definition of drizzling status follows the

397   method in Wu et al., (2015, 2017) where there are radar reflectivity measurements below the

398   ceilometer/lidar determined cloud base. The major difference for drizzles in the studies of Wu et

399   al. (2015, 2017) and this study is that drizzle is liquid phase at ARM ENA site but could be both

400   liquid and ice phases in this study.

401   The percentages shown below the x-axis represent the portion of drizzling status in each type

402   of clouds, such as liquid, mixed-phase, ice and 'OTHER' clouds. Figure 7 (bottom panel) also

403   shows the percentages and vertical distributions of classified liquid, mixed-phase, ice, and

404   'OTHER' clouds for each column in the single-layered low-level clouds, represented by different

405   colors. After classification, the samples in each category are sorted by their H_{top}. In detail, Figure

406   7 demonstrates that the mixed-phase clouds dominate the single-layered low-level cloud category

407   with an occurrence frequency of 54.5 %. The 'OTHER' and ice clouds have similar occurrence

408   frequencies of 18.1 % and 17.4 %, respectively, while the liquid clouds have the lowest occurrence

409   frequency of 10.1 %. The liquid-topped mixed-phase clouds (included in 'OTHER'), which

410   frequently occur in the Arctic region (Qiu et al., 2015), are rarely found over the SO. The existence

411   of ice particles in mixed-phase clouds should strongly depend on the distribution of ice nuclei (IN),

412   whereas spatially unevenly distributed IN may result in the OTHER type of clouds.

413   Based on the results in Fig. 7, we draw the following conclusions. Most of the ice clouds are

414   without icy precipitation, and the percentages with virga and precipitation below the cloud base

415   are 12 %, and 15 %, respectively. The percentages of non-drizzling, virga and drizzling mixed-

416   phase clouds are 50 %, 21 %, and 29 %. The liquid and 'OTHER' clouds have similar percentages,

417   they are 36 %, 25 % and 39 % for liquid clouds, and 35 %, 22 % and 44 % for 'OTHER' clouds.

418   For liquid and 'OTHER' clouds, the drizzling frequencies are independent of H_{top}. In contrast, for

419   mixed-phase and ice clouds, the drizzling frequencies strongly depend on H_{top}, i.e., higher drizzling

420   frequencies occur mostly at higher H_{top}.

421   The properties of single-layered low-level clouds are summarized in Table 4. The liquid clouds

422   have the lowest H_{base} and H_{top} but more available water vapor than other types of clouds. Since the

423   'OTHER' clouds are a transitional stage among mixed-phase, liquid and ice clouds, they have the

424   highest H_{top}, deepest cloud layer and largest *LWP*. The ice clouds occur in relatively dry

425   environments and have the highest H_{base} at 1.218 km and thinnest cloud layer. The cloud variables

426   for mixed-phase clouds fall between Liquid and "OTHER". Since *LWP*s in mixed-phase clouds

427   have larger standard deviation, which implies that SLW is more common at higher *LWP*s and ice

428   is more common at lower *LWP*s.

429   **4.2. Meridional variations of cloud properties**

430   Figure 8 shows the meridional variation in single-layered low-level cloud properties during

431   MARCUS. As illustrated in Fig. 8a, the meridional distributions of H_{base}, H_{top} and ΔH are nearly

432   independent of latitude, however, their corresponding temperatures (T_{base} and T_{top}) increased about

433   8 K from 69 °S to 43 °S, though there were slight fluctuations. These results suggest that the cloud

434   and sea surface temperatures have minimal impact on the cloud boundaries over the SO, which is

435   consistent with the findings in McFarquhar et al. (2016). The meridional variation of *LWP*s follows

436   those of T_{base} and T_{top}, with an increasing trend from south to north. It is important to point out that

437   a big drop in *LWP* at ~50 ºS results from fewer occurrences of low-level clouds there, indicating

438   that the cloud samples at some latitudes are not statistically significant. The atmospheric *PWV*

439   increased dramatically from ~ 5 mm at 69 °S to ~18 mm at 43 °S, presumably due to increased sea

440   surface and atmospheric temperatures.

441   Figure 9 shows the latitudinal and meridional distributions of categorized liquid, mixed-phase,

442   ice and 'OTHER' in single-layered low-level clouds over the SO during MARCUS. Each circle

443   represents the exact location and time along the ship track. Mixed-phase clouds occurred

444   everywhere over the SO during the MARCUS field campaign and became dominant in November,

445   December and February. Liquid clouds dominated in March, while ice clouds dominated in

446   January. The 'OTHER' clouds are a kind of transitional phase falling in between the mixed-phase

447   and ice/liquid clouds because there are no stand-alone occurrences in any month during MARCUS.

448   **4.3 Vertical distribution of cloud properties**

449   The vertical distributions of classified liquid, mixed-phase, and ice clouds in LOW category

450   are presented in Figs. 10-12. The focus of this section will be comparisons of cloud macrophysical

451   properties between the north (NSO) and south (SSO) regions of the domain. Figure 10a shows the

452   vertical distributions of liquid clouds, which were capped at ~ 1.6 km, mostly in the marine

453   boundary layer. The vertical occurrence frequencies are up to 27 % over NSO, while they were

454   less than 4 % over SSO, i.e., liquid clouds occurred fairly often over the mid-latitude region, but

455   very few occurred over the Polar region. On the contrary, the occurrence frequencies of mixed-

456   phase clouds between NSO and SSO are opposite to liquid clouds as illustrated in Fig. 10b, though

457   the differences are not so obvious. Mixed-phase clouds increased with altitude until ~1.6 km, then

458   decreased monotonically towards 3 km. The highest frequencies were ~37 % at 0.6 km over SSO

459   and ~27 % at 1.5 km over NSO. The vertical distributions of ice clouds are similar to those of

460   mixed-phase clouds (Fig. 10c), however, there were no significant differences between NSO and

461   SSO. It is worth mentioning that the vertical distributions of mixed-phased clouds over SO are

462   quite different to those from DOE ARM Northern Slope Alaska (NSA) site, where the low-level

463   mixed-phase clouds are commonly featured with a liquid-topped layer. (e.g., Qiu et al., 2015).

464   To further investigate the vertical distributions of classified liquid, mixed-phase, and ice clouds

465   over NSO and SSO, we plot the normalized vertical distributions (cloud base as 0, cloud top as 1)

466   of radar reflectivity, Doppler velocity and spectrum width in Figs. 11 and 12, respectively. In this

467   study, the threshold of -50 dBZ was used to determine the cloud boundary over the SO instead of

468   the threshold of -40 dBZ radar reflectivity used at the ARM ENA site (Dong et al., 2014). If we

469   used the threshold of -40 dBZ over the SO, then there would be only 73% cloud samples available.

470   If we used the threshold of -50 dBZ, then we would have 90.4% cloud samples, which gained

471   additional 17.4% on top of the -40 dBZ threshold. About 9.6% of radar reflectivities during

472   MARCUS are lower than -50 dBZ for all LOW cloud samples, but without ceilometer and MPL

473   lidar signials. Thus these 9.6% cloud samples were eliminated in Figs 11-12.

474   Figures 11a-11c represent the normalized vertical distributions of radar reflectivity, Doppler

475   velocity and spectrum width of liquid clouds. Liquid clouds had the lowest reflectivity near the

476   cloud top because of cloud-top entrainment., The reflectivity had a nearly constant median value

477   of ~ -22 dBZ from cloud top height (~ 0.8 for normalized height) of the cloud layer to the cloud

478   base. Most of the reflectivities were less than -15 dBZ, which is a threshold to distinguish cloud

479   droplets and drizzle drops in each radar range volume (Wu et al., 2020). Most of the Doppler

480   velocities were greater than 0.0 m s^{-1}, indicating that downwelling motion is dominant in liquid

481   clouds. The profiles of Doppler velocity and spectrum width increased smoothly from the cloud

482   top to base, suggesting that larger cloud droplets and broader size distributions exist near the cloud

483   base, which is attributable to more drizzle drops near the cloud base as illustrated in Fig. 7.

484   The vertical distributions of mixed-phase clouds in Figs. 11d-11f are similar to those of liquid

485   clouds. The more occurrences of larger reflectivity measurements and larger median values of

486   spectrum width near the cloud base are most likely due to the presence of moderate ice particles

487   and/or drizzle drops. The nearly same median values of reflectivity, Doppler velocity and spectrum

488   width (but slightly larger standard deviations in each level in mixed-phase clouds) in both liquid

489   and mixed-phase clouds suggest that the ice particle sizes in mixed-phase clouds are comparable

490   to cloud droplets and drizzle drops. The nearly uniform vertical distributions of Doppler velocity

491   and spectrum width indicate well-mixed liquid cloud droplets and ice particles throughout the

492   cloud layer in the mixed-phase clouds over NSO.

493   Compared to liquid and mixed-phase clouds, ice clouds had much lower reflectivities and

494   narrower spectrum width as shown in Figs. 11g-11i. Almost all reflectivity measurements were

495   less than -25 dBz with a median value of -35 dBz at the cloud base, resulting from small or

496   moderate ice particles but much lower concentration. A nearly constant Doppler velocity within

497   the cloud layer further supports the discussion of mixed-phase clouds above, i.e., the ice particle

498   sizes are independent of cloud height and comparable to liquid cloud droplets in the low-level

499   clouds over the SO. Because there are no mechanisms for growing large ice particles in such

500   shallow ice clouds, the accretion process cannot take place. From the statistical results in Fig. 7,

501   these ice particles have relatively little chance to become virga or raindrops and usually dissipate

502   or transition to other types of clouds.

503   Since there are not enough liquid cloud samples over the Polar region, only the mixed-phase

504   and ice clouds results are shown in Fig. 12. Compared to the vertical distributions of ice clouds

505   over NSO, the median values of reflectivity and Doppler spectrum width over SSO were lower

506   and narrower, indicating a lack of large ice particles in the Polar region. The small ice particles in

507   the Polar region were also reflected in their mixed-phase clouds. Compared to the vertical

508   distributions of the mixed-phased clouds over NSO, the median values of reflectivity and Doppler

509   spectrum width over SSO were dramatically lower (-35 dBz at SSO vs. -22 dBz at NSO; 0.25 m

510   s^{-1} at SSO vs. 0.32 m s^{-1} at NSO). Figure 12 illustrates that the ice particle sizes over SSO are

511   smaller, their size distributions are narrower than those over NSO, indicative of lack of large ice

512   particles over SSO.

513   **5. Summary and Conclusions**

514   In this study, we presented the statistical results of clouds over the Southern Ocean (SO), and

515   its northern (NSO) and southern (SSO) parts during MARCUS Intensive observational period

516   (IOP). We used the method developed in Xi et al., (2010) to calculate the occurrence frequencies

517   of different types of clouds and their corresponding cloud macrophysical properties. We developed

518   a new method to classify liquid, mixed-phased, and ice clouds in the single-layered low-level

519   clouds as well as their corresponding drizzling status. Lastly, we explored the meridional and

520   vertical distributions of these classified cloud properties. Analysis of the MARCUS cloud phase

521   and macrophysical properties has yielded the following conclusions.

522   1) The total cloud fractions (*CF*s) were 77.9 %, 67.6 %, and 90.3 % for the entire domain, NSO

523   and SSO, respectively, indicating that 22.7 % more clouds occurred in the Polar region than in

524   the mid-latitude region. The SSO had more clouds under 7 km, while the NSO had more clouds

525   above 7 km. Below 3 km, the occurrence frequencies of clouds over NSO decrease

526   dramatically from 37 % at an altitude of ~0.7 km to 16 % at 3 km, which is similar to the

527   vertical distributions of the low-level clouds over some Northern Hemisphere mid-latitude

528   regions, such as Eastern North Atlantic.

529 2) The single-layered low-level (LOW), deep connective or multi-layered (HML), and MOL

530   clouds are the three dominant types of clouds over the SO. Comparing the clouds between

531   NSO and SSO, all types of clouds in SSO are higher than those in NSO except HOL. The LOW

532   fraction, thickness, LWP over both NSO and SSO are comparable to each other. The mean

533   *LWP*s for LOW, MID and HOL clouds over NSO, range from ~130 to 150 g m^{-2}, while the

534   mean NSO *LWP*s (~270 g m^{-2}) for MOL and deep convective clouds (HML) are two times

535   higher than the same types of clouds over SSO. The mean *LWP*s of clouds over SSO are much

536   lower than the *LWP*s over NSO. Over the Southern Ocean, the single-layered or contiguous

537   clouds usually have higher LWP than their counterparts of multi-layered or non-contiguous

538   clouds. There are more non-contiguous HML and HOM than contiguous ones.

539 3) A new method was developed to classify liquid, mixed-phase and ice clouds in the single-

540   layered low-level clouds (LOW) based on comprehensive ground-based observations. The

541   mixed-phase clouds are dominant in the LOW cloud category with an occurrence frequency of

542   54.5 %. The 'OTHER' and ice clouds had similar occurrence frequencies of 18.1 % and 17.4 %,

543   respectively, while the liquid clouds had the least occurrence frequency of 10.1 %. The

544   percentages of non-drizzling, virga and drizzling for mixed-phase clouds were 50 %, 21 %,

545   and 29 %, and the drizzling frequencies of mixed-phase clouds strongly depend on H_{top}, that

546   is, higher drizzling frequencies occurred mostly at higher H_{top}.

547 4) The meridional distributions of H_{base}, H_{top} and ΔH are nearly independent on latitude, however,

548   their corresponding temperatures increased about 8 K from 69 $^{\circ}$S to 43 $^{\circ}$S. The meridional

549   variation of *LWP*s mimics that of cloud temperatures, having an increasing trend from south

550   to north. The mean *PWV* increased dramatically from ~ 5 mm at 69 °S to ~18 mm at 43 °S due

551   to increased sea surface and atmospheric temperatures. More liquid clouds occurred over NSO

552   but very few occurred over SSO, whereas more mixed-phase clouds occurred over SSO than

553   over NSO. There were no significant differences in ice clouds occurrences between NSO and

554   SSO.

555 5) The nearly same median values of reflectivity, Doppler velocity and spectrum width in both

556   liquid and mixed-phase clouds over NSO suggest that the ice particle sizes in mixed-phase

557   clouds are comparable to cloud droplets and drizzle drops. The uniform vertical distributions

558   of Doppler velocity and spectrum width suggest well-mixed liquid cloud droplets and ice

559   particles throughout the cloud layer in the mixed-phase clouds over NSO, which are quite

560   different from those over the DOE ARM NSA site where the liquid-topped mixed-phase low-

561   level clouds are common. The median values of reflectivity and Doppler spectrum width over

562   SSO were lower and narrower than those over NSO, indicating lack of large ice particles in

563   the polar region.

564   These results provide comprehensive statistical properties of all clouds over the SO during

565   MARCUS, including the occurrence frequencies of different types of clouds and their

566   corresponding cloud macrophysical properties. We also examined the meridional and vertical

567   distributions of the classified cloud properties. These statistics can be used as a ground truth to

568   evaluate satellite retrieved cloud properties and model simulations over the SO. The results of this

569   study will help to advance our understanding of the clouds over the SO, which may lead to

570   improved model simulations, as well as better representation of global climate.

571   *Data availability.* Data used in this study can be accessed from the DOE ARM's Data Discovery at

572   https://adc.arm.gov/discovery/

573

574   *Author contributions.* The idea of this study is discussed by BX, XD, and XZ. BX and XZ performed

575   the analyses and BX wrote the manuscript. BX, XD, XZ and PW participated in scientific discussions

576   and provided substantial comments and edits on the paper.

577

578   *Competing interests.* The authors declare that they have no conflict of interest.

579

580   *Acknowledgements.* The ground-based measurements were obtained from the Atmospheric

581   Radiation Measurement (ARM) Program sponsored by the U.S. Department of Energy (DOE)

582   Office of Energy Research, Office of Health and Environmental Research, and Environmental

583   Sciences Division. The data can be downloaded from http://www.archive.arm.gov/. Researchers

584   were supported by the NSF project under grant AGS-2031750 at the University of Arizona.

585   Specially thanks to Mr. Xingyu Zhang for providing analysis from CDP and 2DS microphysical

586   sensors during SOCRATES and Dr. Dale Ward for proofreading this manuscript.

587 **References.**

588 Albrecht, B. A.: Aerosols, cloud microphysics, and fractional cloudiness, Science,

589   doi:10.1126/science.245.4923.1227, 1989.

590 Bodas-Salcedo, A., Mulcahy, J. P., Andrews, T., Williams, K. D., Ringer, M. A., Field, P. R. and

591   Elsaesser, G. S.: Strong Dependence of Atmospheric Feedbacks on Mixed-Phase

592   Microphysics and Aerosol-Cloud Interactions in HadGEM3, J. Adv. Model. Earth Syst.,

593   doi:10.1029/2019MS001688, 2019.

594 Bony, S., Stevens, B., Frierson, D. M. W., Jakob, C., Kageyama, M., Pincus, R., Shepherd, T. G.,

595   Sherwood, S. C., Siebesma, A. P., Sobel, A. H., Watanabe, M. and Webb, M. J.: Clouds,

596   circulation and climate sensitivity, Nat. Geosci., doi:10.1038/ngeo2398, 2015.

597 Chubb, T. H., Jensen, J. B., Siems, S. T. and Manton, M. J.: In situ observations of supercooled

598   liquid clouds over the Southern Ocean during the HIAPER Pole-to-Pole Observation

599   campaigns, Geophys. Res. Lett., doi:10.1002/grl.50986, 2013.

600 Dong, X., Xi, B., Kennedy, A., Minnis, P. and Wood, R.: A 19-month record of marine aerosol-

601   cloud-radiation properties derived from DOE ARM mobile facility deployment at the

602   Azores. Part I: Cloud fraction and single-layered MBL cloud properties, J. Clim.,

603   doi:10.1175/JCLI-D-13-00553.1, 2014.

604 Hu, Y., Rodier, S., Xu, K. M., Sun, W., Huang, J., Lin, B., Zhai, P. and Josset, D.: Occurrence,

605   liquid water content, and fraction of supercooled water clouds from combined

606   CALIOP/IIR/MODIS   measurements,   J.   Geophys.   Res.   Atmos.,

607   doi:10.1029/2009JD012384, 2010.

608   Intrieri, J. M., Fairall, C. W., Shupe, M. D., Persson, P. O. G., Andreas, E. L., Guest, P. S. and

609   Moritz, R. E.: An annual cycle of Arctic surface cloud forcing at SHEBA, J. Geophys. Res.

610   Ocean., doi:10.1029/2000jc000439, 2002.

611   Klein, S. A., Hall, A., Norris, J. R. and Pincus, R.: Low-Cloud Feedbacks from Cloud-Controlling

612   Factors: A Review, Surv. Geophys., doi:10.1007/s10712-017-9433-3, 2017.

613   Kalesse, H., de Boer, G., Solomon, A., Oue, M., Ahlgrimm, M., Zhang, D., Shupe, M. D., Luke,

614   E. and Protat, A.: Understanding rapid changes in phase partitioning between cloud liquid

615   and ice in stratiform mixed-phase clouds: An arctic case study, Mon. Weather Rev.,

616   doi:10.1175/MWR-D-16-0155.1, 2016.

617   Lang, F., Huang, Y., Siems, S. T. and Manton, M. J.: Characteristics of the Marine Atmospheric

618   Boundary Layer Over the Southern Ocean in Response to the Synoptic Forcing, J. Geophys.

619   Res. Atmos., doi:10.1029/2018JD028700, 2018.

620   Listowski, C., Delanoë, J., Kirchgaessner, A., Lachlan-Cope, T. and King, J.: Antarctic clouds,

621   supercooled liquid water and mixed phase, investigated with DARDAR: Geographical and

622   seasonal variations, Atmos. Chem. Phys., doi:10.5194/acp-19-6771-2019, 2019.

623   Mace, G. G., Zhang, Q., Vaughan, M., Marchand, R., Stephens, G., Trepte, C. and Winker, D.: A

624   description of hydrometeor layer occurrence statistics derived from the first year of merged

625   Cloudsat and CALIPSO data, J. Geophys. Res. Atmos., doi:10.1029/2007JD009755, 2009.

626   Mace, G. G. J. and Protat, A.: Clouds over the Southern Ocean as observed from the R/V

627   investigator during CAPRICORN. Part I: Cloud occurrence and phase partitioning, J. Appl.

628   Meteorol. Climatol., doi:10.1175/JAMC-D-17-0194.1, 2018.

629   Mace, G. G., Protat, A., Humphries, R. S., Alexander, S. P., McRobert, I. M., Ward, J., Selleck,

630   P., Keywood, M. and McFarquhar, G. M.: Southern Ocean Cloud Properties Derived From

631   CAPRICORN and MARCUS Data, J. Geophys. Res. Atmos., doi:10.1029/2020JD033368,

632   2021.

633 Marchand, R., Ackerman, T., Westwater, E. R., Clough, S. A., Cady-Pereira, K. and Liljegren, J.

634   C.: An assessment of microwave absorption models and retrievals of cloud liquid water

635   using clear-sky data, J. Geophys. Res. Atmos., doi:10.1029/2003jd003843, 2003.

636 Marchand, R., Wood, R., Bretherton, C., McFarquhar, G., Protat, A., Quinn, P., Siems, S., Jakob,

637   C., Alexander, S., Weller, B.: The Southern Ocean Clouds, Radiation Aerosol Transport

638   Experimental   Study   (SOCRATES),   whitepaper   available   from

639   http://www.atmos.washington.edu/socrates/SOCRATES_white_paper_Final_Sep29_201

640   4.pdf, 2014.

641 Mccoy, D. T., Hartmann, D. L. and Grosvenor, D. P.: Observed Southern Ocean cloud properties

642   and shortwave reflection. Part II: Phase changes and low cloud feedback, J. Clim.,

643   doi:10.1175/JCLI-D-14-00288.1, 2014.

644 McFarquhar, G., Bretherton, C., Alexander, S., DeMott, P., Marchand, R., Protat, A., Quinn, P.,

645   Siems, S., Weller, R., Wood, R.: Measurements of Aerosols, Radiation, and Clouds over

646   Sothern Ocean (MARCUS) Science Plan, DOE ARM Climate Research Facility.,

647   DOE/SC-ARM-16-011,   available   at: http://arm.gov/publications/programdocs/doe-sc-

648   arm-16-011.pdf, 2016.

649 McFarquhar, G. M., Bretherton, C. S., Marchand, R., Protat, A., DeMott, P. J., Alexander, S. P.,

650   Roberts, G. C., Twohy, C. H., Toohey, D., Siems, S., Huang, Y., Wood, R., Rauber, R. M.,

651   Lasher-Trapp, S., Jensen, J., Stith, J. L., Mace, J., Um, J., Järvinen, E., Schnaiter, M.,

652   Gettelman, A., Sanchez, K. J., McCluskey, C. S., Russell, L. M., McCoy, I. L., Atlas, R.

653   L., Bardeen, C. G., Moore, K. A., Hill, T. C. J., Humphries, R. S., Keywood, M. D.,

654   Ristovski, Z., Cravigan, L., Schofield, R., Fairall, C., Mallet, M. D., Kreidenweis, S. M.,

655   Rainwater, B., D'Alessandro, J., Wang, Y., Wu, W., Saliba, G., Levin, E. J. T., Ding, S.,

656   Lang, F., Truong, S. C. H., Wolff, C., Haggerty, J., Harvey, M. J., Klekociuk, A. R., and

657   McDonald, A.: Observations of Clouds, Aerosols, Precipitation, and Surface Radiation

658   over the Southern Ocean: An Overview of CAPRICORN, MARCUS, MICRE, and

659   SOCRATES, B. Am. Meteorol. Soc., 102, E894-E928, 10.1175/BAMS-D-20-0132.1,

660   2021.

661 Mohrmann, J., Finlon, J., Atlas, R., Lu, J., Hsiao, I., Wood, R.: University of Washington Ice-

662   Liquid Discriminator single particle phase classifications and 1 Hz particle size

663   distributions/heterogeneity estimate, Version 1.0. UCAR/NCAR - Earth Observing

664   Laboratory., doi:10.26023/PA5W-4DRX-W50A, Last Access: Nov 01, 2021

665 Morrison, H., De Boer, G., Feingold, G., Harrington, J., Shupe, M. D. and Sulia, K.: Resilience of

666   persistent Arctic mixed-phase clouds, Nat. Geosci., doi:10.1038/ngeo1332, 2012.

667 Muradyan, P. and Coulter, R.: Micropulse Lidar (MPL) Instrument Handbook. DOE ARM Climate

668   Research   Facility,   DOE/SC-ARM-TR-019,   2020.   Available   at:

669   https://www.arm.gov/publications/tech_reports/handbooks/mpl_handbook.pdf, last access:

670   25 March 2022.

671 Qiu, S., Dong, X., Xi, B. and Li, J. L. F.: Characterizing Arctic mixed-phase cloud structure and

672   its relationship with humidity and temperature inversion using ARM NSA observations, J.

673   Geophys. Res., doi:10.1002/2014JD023022, 2015.

674 Rémillard, J., Kollias, P., Luke, E., and Wood, R.: Marine Boundary Layer Cloud Observations in

675   the Azores, J. Climate, 25, 7381-7398, 10.1175/JCLI-D-11-00610.1, 2012.

676   Sassen, K.: The polarization lidar technique for cloud research: a review and current assessment,

677   Bull. - Am. Meteorol. Soc., doi:10.1175/1520-0477(1991)072<1848:TPLTFC>2.0.CO;2,

678   1991.

679   Shupe, M. D., Uttal, T. and Matrosov, S. Y.: Arctic cloud microphysics retrievals from surface-

680   based remote sensors at SHEBA, J. Appl. Meteorol., doi:10.1175/JAM2297.1, 2005.

681   Shupe, M.: A ground-based multisensory cloud phase classifier, Geophys. Res. Lett.,

682   doi:10.1029/2007GL031008, 2007.

683   Stanfield, R. E., Dong, X., Xi, B., Kennedy, A., Del Genio, A. D., Minnis, P. and Jiang, J. H.:

684   Assessment of NASA GISS CMIP5 and Post-CMIP5 Simulated Clouds and TOA

685   Radiation Budgets Using Satellite Observations. Part I: Cloud Fraction and Properties, J.

686   Clim., doi:10.1175/jcli-d-13-00558.1, 2014.

687   Stanfield, R. E., Dong, X., Xi, B., Del Genio, A. D., Minnis, P., Doelling, D. and Loeb, N.:

688   Assessment of NASA GISS CMIP5 and post-CMIP5 simulated clouds and TOA radiation

689   budgets using satellite observations. Part II: TOA radiation budget and CREs, J. Clim.,

690   doi:10.1175/JCLI-D-14-00249.1, 2015.

691   Stocker, T. F., Qin, D., Plattner, G. K., Tignor, M. M. B., Allen, S. K., Boschung, J., Nauels, A.,

692   Xia, Y., Bex, V. and Midgley, P. M.: Climate change 2013 the physical science basis:

693   Working Group I contribution to the fifth assessment report of the intergovernmental panel

694   on climate change., 2013.

695   Toto, T. and Jensen, M.: Interpolated Sounding and Gridded Sounding Value-Added Products.

696   DOE ARM Climate Research Facility, DOE/SC-ARM-TR-183, 2016. Available at:

697   https://www.arm.gov/publications/tech_reports/doe-sc-arm-tr-183.pdf, last access: 25

698   March 2022.

699   Uin, J.: Cloud Condensation Nuclei Particle Counter Instrument Handbook. DOE ARM Climate

700   Research   Facility,   DOE/SC-ARM-TR-168,   2016.   Available   at:

701   https://www.arm.gov/publications/tech_reports/handbooks/ccn_handbook.pdf, last access:

702   25 March 2022.

703   Wu, P., Dong, X. and Xi, B.: Marine boundary layer drizzle properties and their impact on cloud

704   property retrieval, Atmos. Meas. Tech., doi:10.5194/amt-8-3555-2015, 2015.

705   Wu, P., Dong, X., Xi, B., Liu, Y., Thieman, M. and Minnis, P.: Effects of environment forcing on

706   marine   boundary   layer   cloud-drizzle   processes,   J.   Geophys.   Res.,

707   doi:10.1002/2016JD026326, 2017.

708   Wu, P., Dong, X. and Xi, B.: A climatology of marine boundary layer cloud and drizzle properties

709   derived from ground-based observations over the azores, J. Clim., doi:10.1175/JCLI-D-20-

710   0272.1, 2020.

711   Xi, B., Dong, X., Minnis, P. and Khaiyer, M. M.: A 10 year climatology of cloud fraction and

712   vertical distribution derived from both surface and GOES observations over the DOE ARM

713   SPG site, J. Geophys. Res. Atmos., doi:10.1029/2009JD012800, 2010.

714   Zelinka, M. D., Myers, T. A., McCoy, D. T., Po-Chedley, S., Caldwell, P. M., Ceppi, P., Klein, S.

715   A. and Taylor, K. E.: Causes of Higher Climate Sensitivity in CMIP6 Models, Geophys.

716   Res. Lett., doi:10.1029/2019GL085782, 2020.

717   Zhao, L., Zhao, C., Wang, Y., Wang, Y. and Yang, Y.: Evaluation of Cloud Microphysical

718   Properties Derived From MODIS and Himawari-8 Using In Situ Aircraft Measurements

719   Over the Southern Ocean, Earth Sp. Sci., doi:10.1029/2020EA001137, 2020.

Table 1. ARM AMF2 instruments and their corresponding measurements and uncertainties used in this study

Parameter	Instruments/ Methods	Uncertainty	References
Cloud-base height	Ceilometer/MPL	15 m	Rémillard et al., 2012
Cloud-top height	95 GHz cloud radar	43 m	Rémillard et al., 2012
Cloud-base and -top temps	Radiosonde sounding	0.2 °C	Toto and Jensen, 2016
Profiles of reflectivity, Doppler velocity and Spectra	W-band ARM Cloud Radar (WACR), 95 GHz	Sensitivity: -50 dBZ at 2 km	Rémillard et al., 2012
linear depolarization ratios (*LDR*) and backscatter	Micropulse lidar, MPL Liquid: LDR<0.11 Mix: 0.11<LDR<0.15 Ice: LDR> 0.15		Shupe et al. 2005 Muradyan and Coulter, 2020
Cloud LWP	Microwave radiometer	~15-30 g m^{-2} Physical retrieval	Marchand et al., 2003
CCN and aerosol properties	Aerosol Observing System	1-min resolution; Uncertainties < 10%	Uin, 2016

Table 2. Mean, standard deviation, minimum and maximum cloud-base heights (H_{base}), -top heights (H_{top}), and *LWP*s (all samples, single-layered, multilayered) of all seven types of clouds over the SO. All cloud heights have a unit of kilometer, and *LWP* has a unit of g m^{-2}

	LOW	MID	MOL	HGH	HOM	HML	HOL
H_{base} ± std	0.92 ± 0.57	4.14 ± 0.61	1.37 ± 0.96	8.51 ± 2.23	4.70 ± 0.80	1.22 ± 0.98	1.14 ± 1.12
min, max	0.06, 2.86	3.00, 5.84	0.06, 5.27	6.00, 18.67	3.01, 7.72	0.06, 7.81	0.07, 10.37
H_{top} ± std	1.62 ± 0.63	4.88 ± 0.68	4.29 ± 0.89	9.75 ± 2.13	7.93 ± 1.27	7.81 ± 1.35	8.93 ± 1.66
min, max	0.29, 3.0	3.17, 6.0	1.39, 5.99	6.20,18.79	5.47, 17.98	3.62,17.38	1.79, 17.56
LWP ± std	122.4 ± 134.2	86.7 ± 124.5	168.7 ± 236.7	/	40.9 ± 40.8	169.2 ± 238.4	$129.8 \pm 202.$
Max *LWP*	1470.8	501.1	1937.1	/	345.7	1819.3	1785.2
LWP ± std (single layer)	126.6 ± 138.1	88.7 ± 128.9	193.1 ± 271.9	/	48.7 ± 51.7	270.8 ± 349.5	/
max	1470.8	501.1	1937.1	/	345.7	1819.3	/
LWP ± std (multi-layer)	96.2 ± 103.4	77.2 ± 109.2	139.0 ± 180.7	/	32.3 ± 21.3	148.4 ± 202.4	$129.8 \pm 202.$
max	842.3	305.6	1830.2	/	86.8	1690.7	1785.2
Multi-layer percentage %	18.1	39.6	50.0	44.9	73.1	77.7	100

* The definition of the cloud types as follow: LOW (H_{base} and $H_{top} \leq 3\ km$); MID ($H_{base} > 3\ km$ and $H_{top} \leq 6\ km$); HGH ($H_{base} > 6\ km$); MOL ($H_{base} < 3\ km$ and $H_{top} \leq 6\ km$); HOM ($3\ km < H_{base} < 6\ km$ and $H_{top} > 6\ km$); HML ($H_{base} < 3\ km$, $H_{top} \geq 6\ km$ with a MID layer); HOL (LOW and HGH appear at the same time).

Table 3a. Comparison of cloud phase identifications between our classification method and Shupe et al. (2005) method in each 5-min measurements, the unit is number of 5-min samples

Shupe \this study	Liquid (this study)	Mixed-phase (this study	Ice (this study)
Liquid	468	490	0
Mixed-phase	98	3840	0
Ice	81	0	1195

*Numbers denote the cloud sample classifications between two methods. For example, the number 98 denote a total of 98 samples are classified as Mixed-phase using Shupe's method, while are classified as Liquid using this study's method.

Table 3b. The cloud phase partitioning from CDP and 2DS during SOCRATES

Phase partitioning	1 second	10 seconds	30 seconds
Samples #	27,280	2,255	836
Liquid, %	58.8	26.2	18.8
Mixed-phase, %	38.9	69.1	77.0
Ice, %	2.3	4.7	4.2

Note that Cloud Droplet Probe (CDP) measures particle size from 2 to 50 um in diameter; Two-Dimensional Stereo Probe (2DS) measures particle size from 50 to 5000 um in diameter.

Table 4. Liquid, mixed, ice and OTHER phases of cloud properties within the single-layered low-level clouds

Phase	Samples	H_{base}, km	H_{top}, km	ΔH, km	LWP, g m^{-2}	PWV, mm
Liquid	697	0.424±0.204	1.327±0.242	0.903	113.6±90.1	15.7±3.5
Mixed	3777	0.834±0.465	1.434±0.617	0.587	119.7±136.6	8.9±5.0
Ice	1205	1.218±0.635	1.737±0.651	0.519	0	8.4±4.5
OTHER	1255	0.700±0.454	1.774±0.571	1.074	141.9±137.5	11.4±5.9
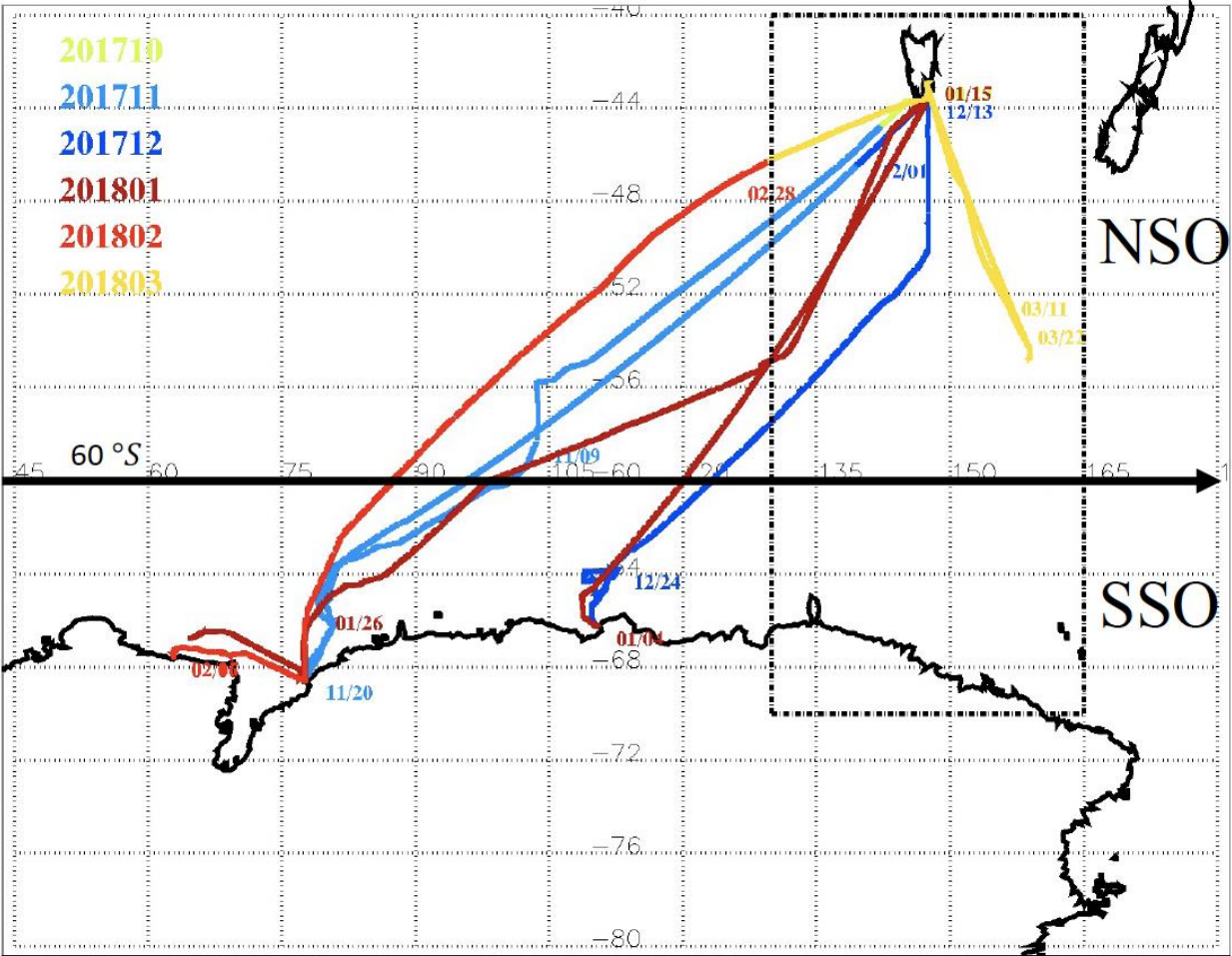
Figure 1. Shiptrack measurements between Hobart, Australia and Antarctica. Different colors represent different month's shiptracks from Oct. 29, 2017 to Mar. 23, 2018 during MARCUS. Along the shiptracks, the study domain is separated into northern (NSO) and southern (SSO) parts of the Southern Ocean with a demarcation line of 60 °S in order to study the clouds over the mid-latitudes (North of 60 °S) and Polar region (South of 60 °S). The black dotted rectangle represents the SOCRATES study domain. Some of the dates are labeled along the shiptracks, indicating the direction of the ship.
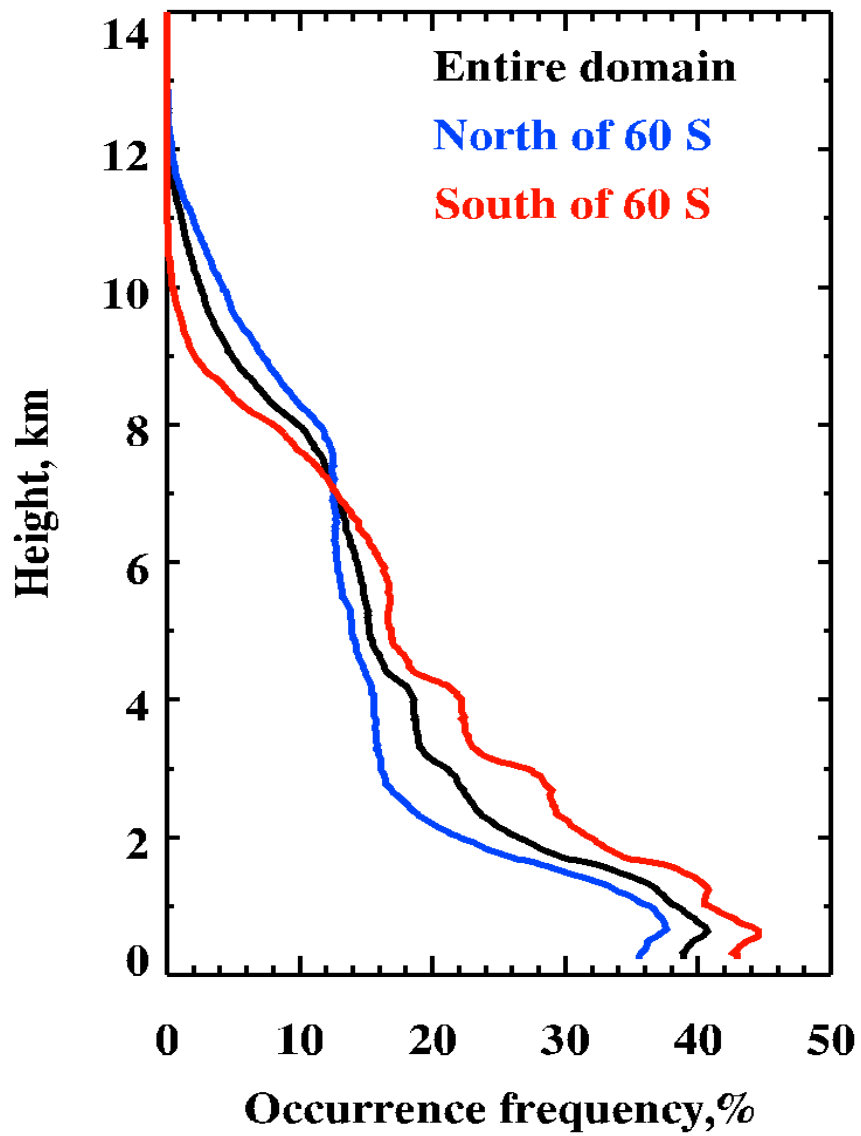
Figure 2. Mean vertical distributions of total clouds derived from ARM radar-lidar observations with a 5-min temporal resolution and a 30-m vertical resolution during MARCUS.
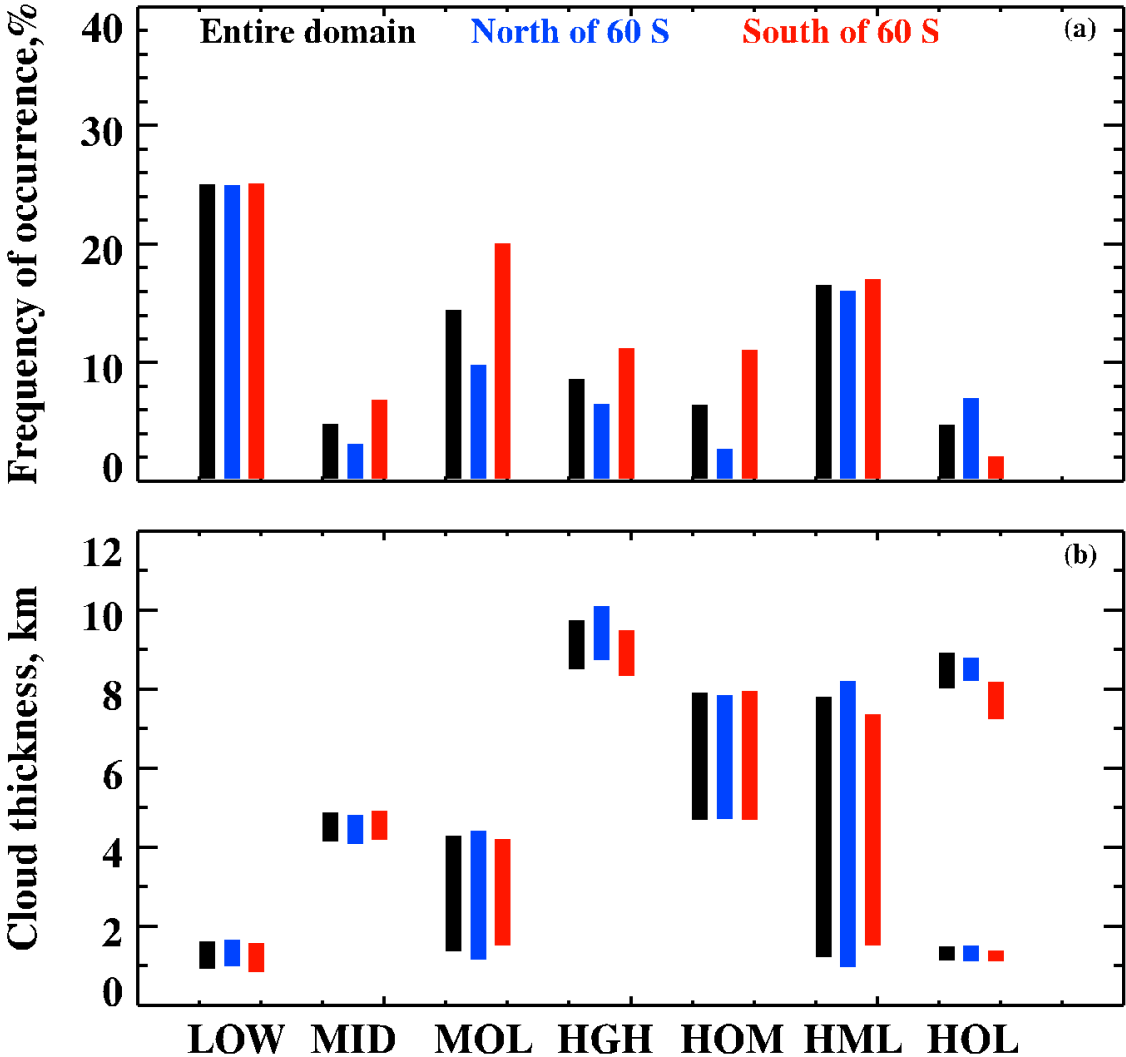
Figure 3. (a) Occurrence frequencies of categorized clouds by their vertical structures. LOW, single‑layered low clouds (H_{base} and $H_{top} \leq 3\ km$); MID, singlelayered middle clouds ($H_{base} > 3\ km$ and $H_{top} \leq 6\ km$); MOL, MID over LOW ($H_{base} < 3\ km$ and $H_{top} \leq 6\ km$); HGH, singlelayered high clouds ($H_{base} > 6\ km$); HOM, HGH over MID ($3\ km < H_{base} < 6\ km$ and $H_{top} > 6\ km$); HML, HGH over MID and LOW ($H_{base} < 3\ km, H_{top} \geq 6\ km$ with a MID layer); and HOL, HGH over LOW (LOW and HGH appear at the same time). (b) Cloud thickness for each type of clouds (bar), the top and bottom of the bar represent the maximum cloud-top and minimum cloud-base heights, respectively. Black, blue, and red bars represent the entire domain (Lat:41-69 °S; Long: 60-160° E), north of 60 °S (NSO), and south of 60°S (SSO), respectively, during the MARCUS field campaign (10/2017-3/2018).
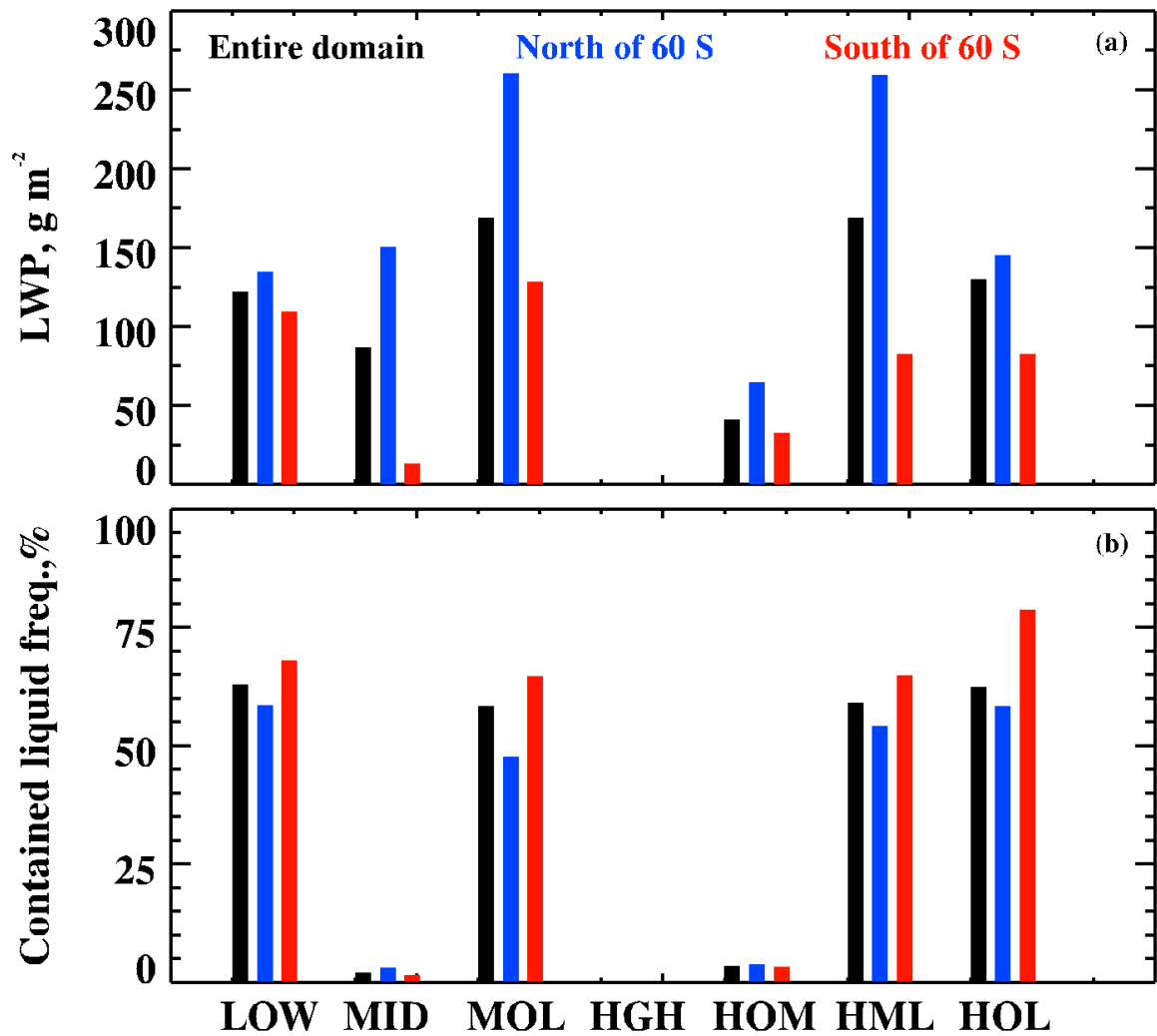
Figure 4. (a) Cloud liquid water paths (*LWP*s) retrieved from microwave radiometer (MWR) measured brightness temperatures using a physical retrieval method for each type of cloud. (b) The occurrence frequencies of LWPs> 10 gm^{-2} for each type of clouds
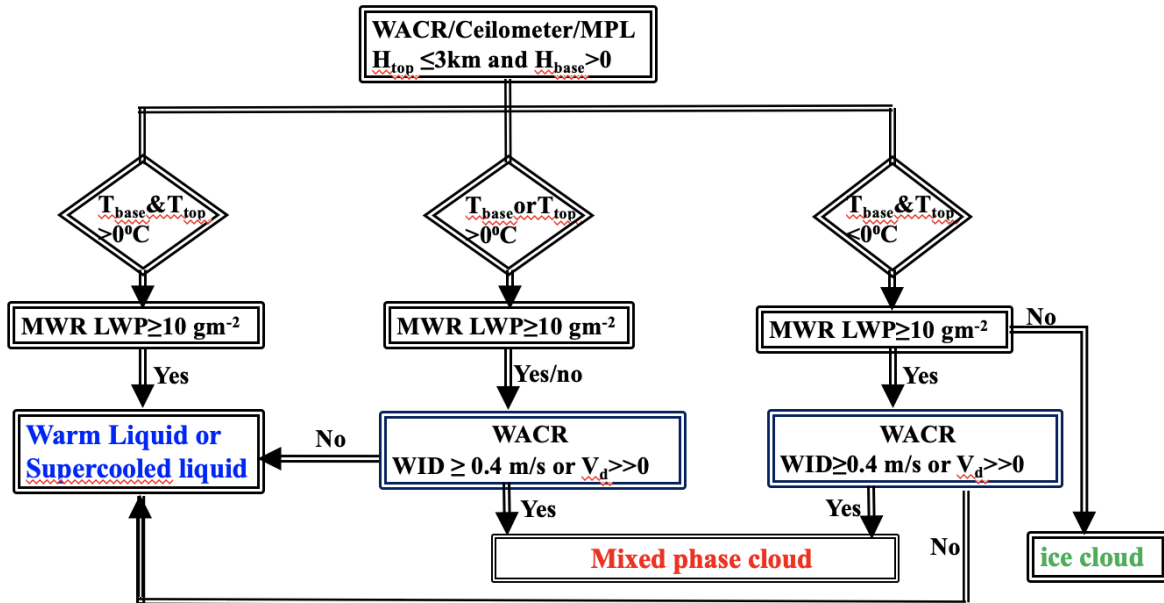
Figure 5. A flow chart for phase classification of single-layered low-level clouds. W-Band (95 GHz) ARM Cloud Radar (WACR) provides radar spectrum width (*WID*) and Doppler velocity (V_d).
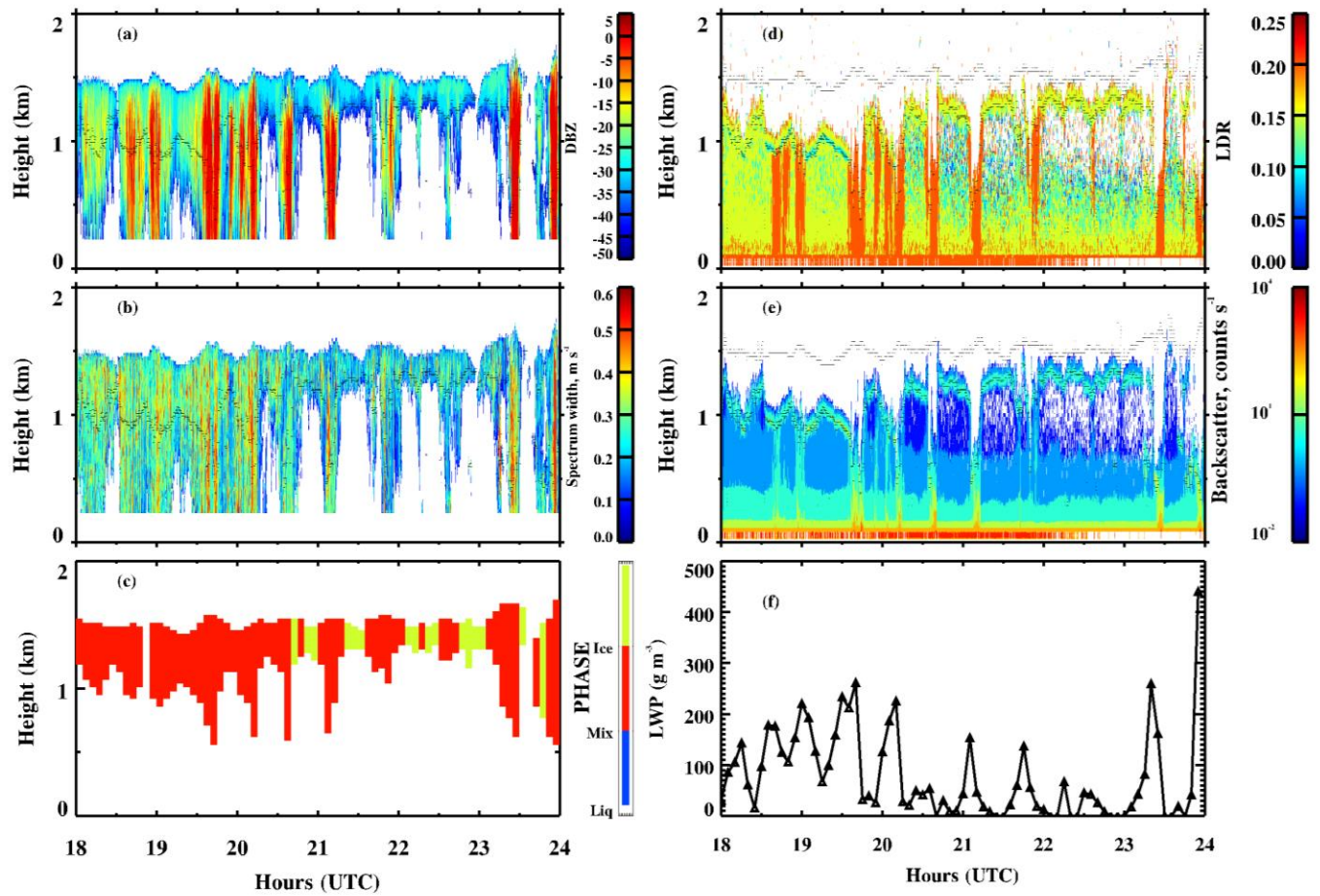
Figure 6. A case study that shows our phase classification (left column) and MicroPulse Lidar (MPL) linear depolarization ratios (*LDR*) and backscatter. W-Band (95 GHz) ARM Cloud Radar (WACR) reflectivity is shown in (a) and spectrum width is shown in (b). Correspondingly, the phase classification in (c); MPL *LDR* in (d) and backscatter in (e); and MWR-derived *LWP* in (f).
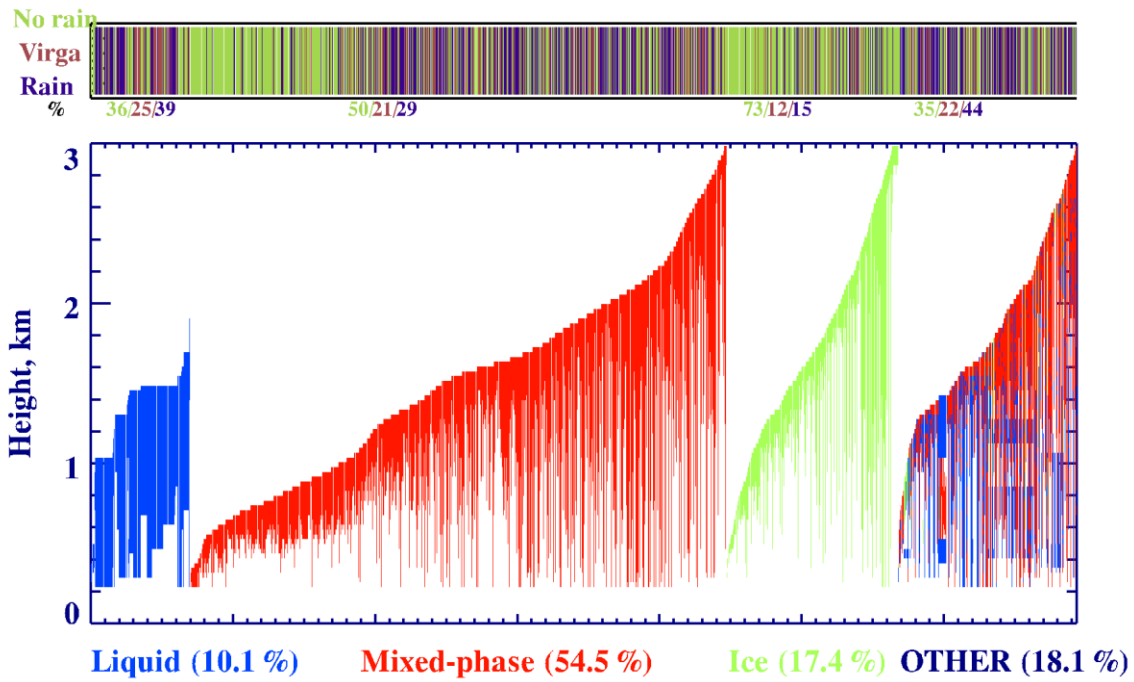
Figure 7. (Upper Panel) The drizzling status for each categorized cloud type, e.g., no rain (yellow-green), virga (brown) and rain (navy blue), the percentages shown below the x-axis represent the portion of drizzling in each type of clouds. (Bottom Panel) The percentages and vertical distributions of classified liquid, mixed-phase, ice, and 'OTHER' clouds for each column in the single-layered low-level clouds, represented by different colors, over the entire domain during MARCUS. Each line represents one 5-min sample. The definition of drizzle here is the radar reflectivity below the ceilometer-derived cloud base, which could be either liquid drizzle drops or ice crystals.
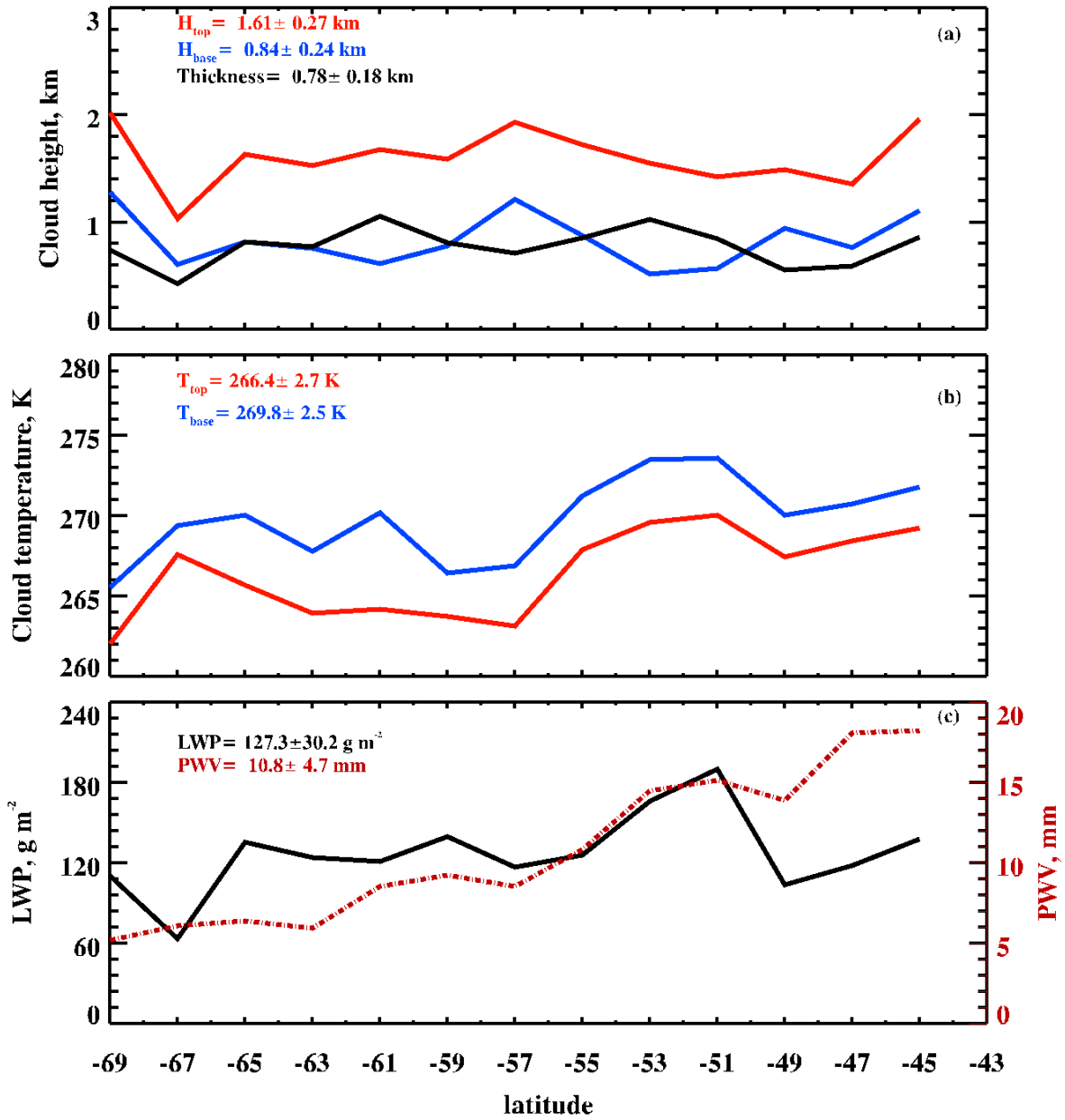
Figure 8. Meridional variations of single-layered low-level cloud properties: (a) cloud-base (H_{base}) and -top (H_{top}) heights, and cloud thickness (ΔH), (b) cloud-base (T_{base}) and -top (T_{top}) temperatures, and (c) cloud liquid water path (*LWP*) and precipitable water vapor (PWV) over the entire domain during MARCUS.
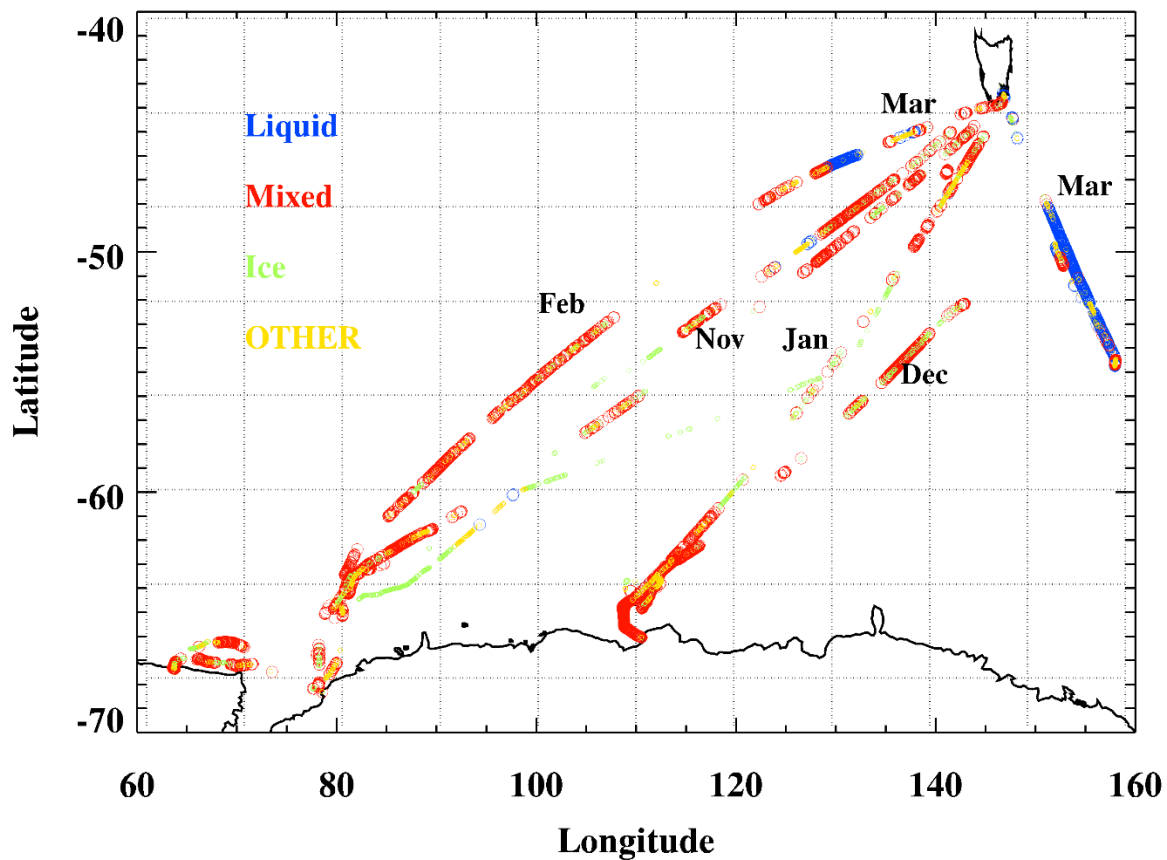
Figure 9. The latitudinal and longitudinal distributions of classified mixed-phase, liquid, and ice clouds in the single-layered low-level clouds. The liquid (blue), mixed (red), ice (light green), and OTHER (yellow) are shown along each shiptrack from October 2017 to March 2018 during MARCUS.
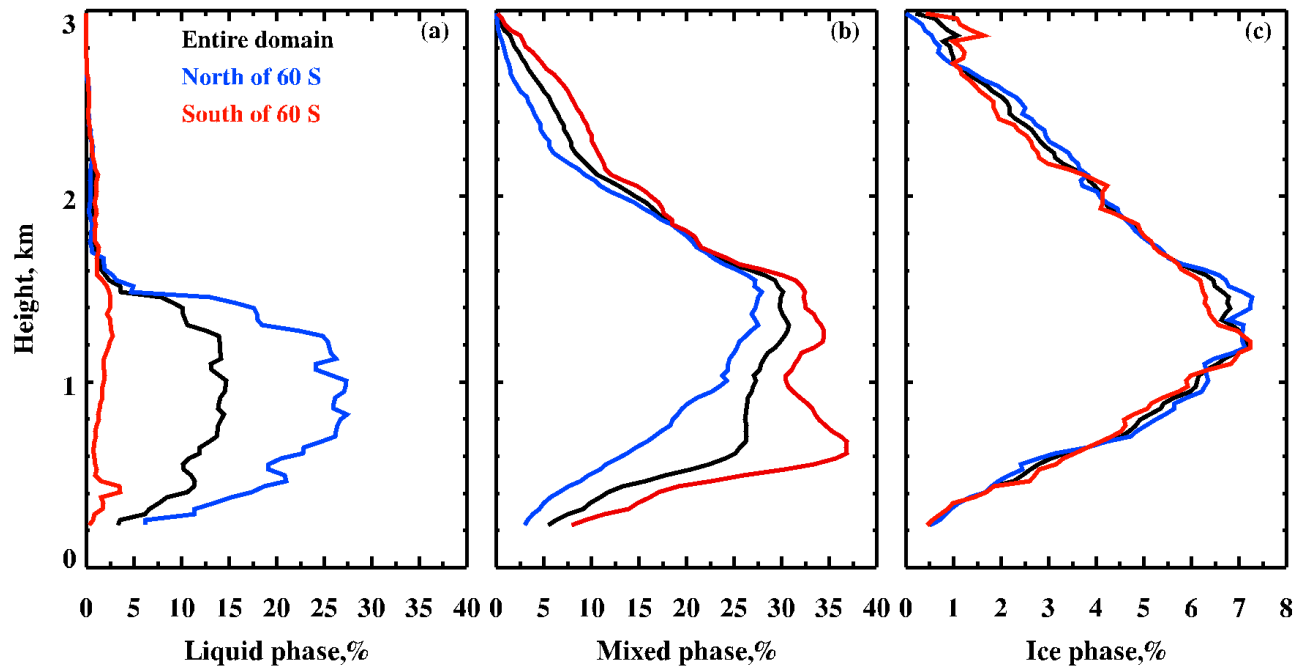
Figure 10. Occurrence frequencies of classified mixed-phase, liquid, and ice clouds over the entire domain (black), North of 60 °S (blue) and South of 60 °S (red) during MARCUS.
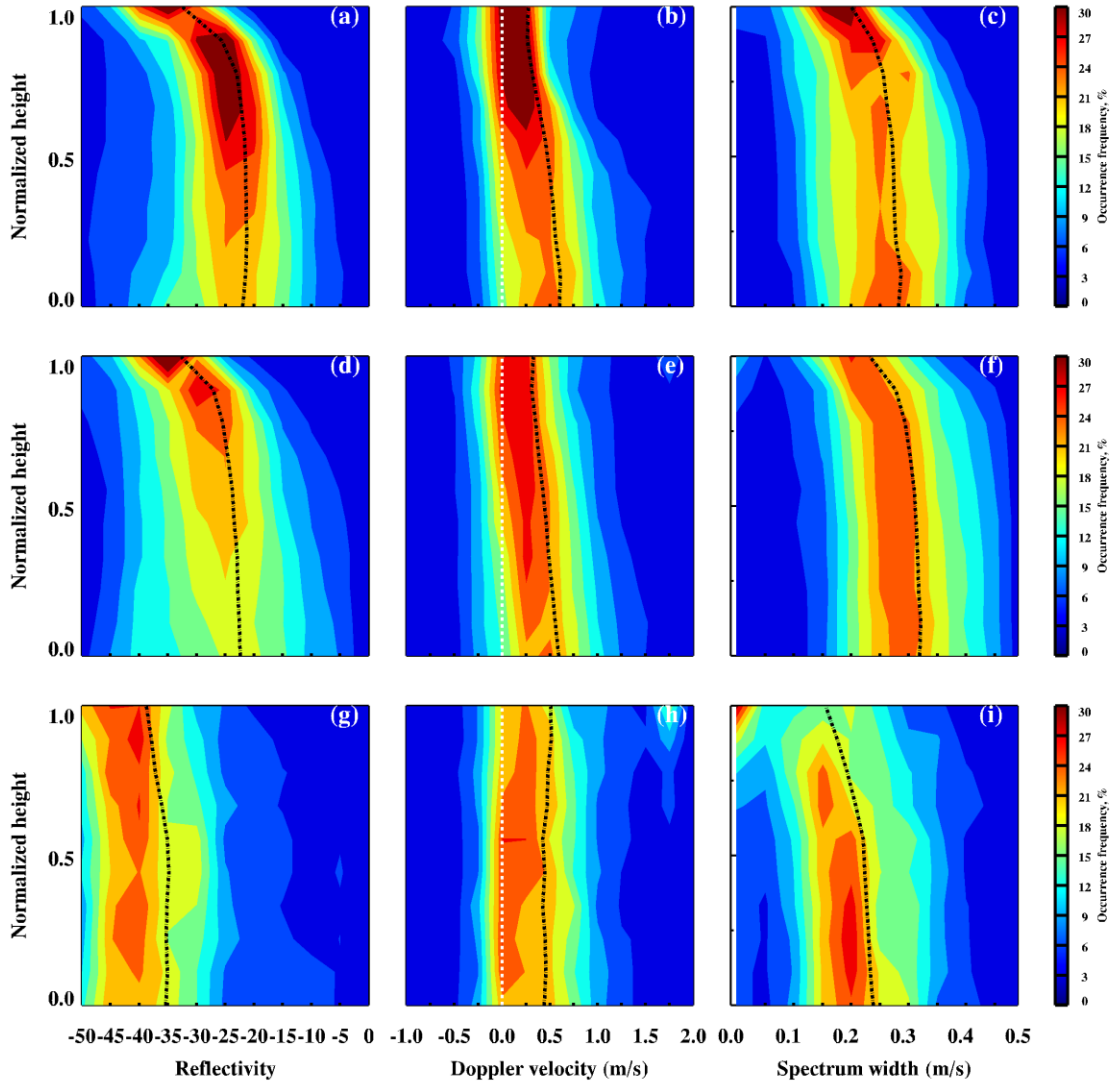
Figure 11. Normalized vertical distributions of radar reflectivity (a), Doppler velocity (b) and spectrum width (c) for the classified liquid (upper panel), mixed-phase (d to f, middle panel) and ice (g to i, bottom panel) clouds over the North of 60 °S during MARCUS Intensive observational period (IOP). Normalized height is defined as $= \frac{H - H_{base}}{H_{top} - H_{base}}$ where cloud base is denoted as 0 and cloud top is 1. The black lines represent the median values and the white lines in Doppler velocity represent the reference of 0.0 m s^{-1}.
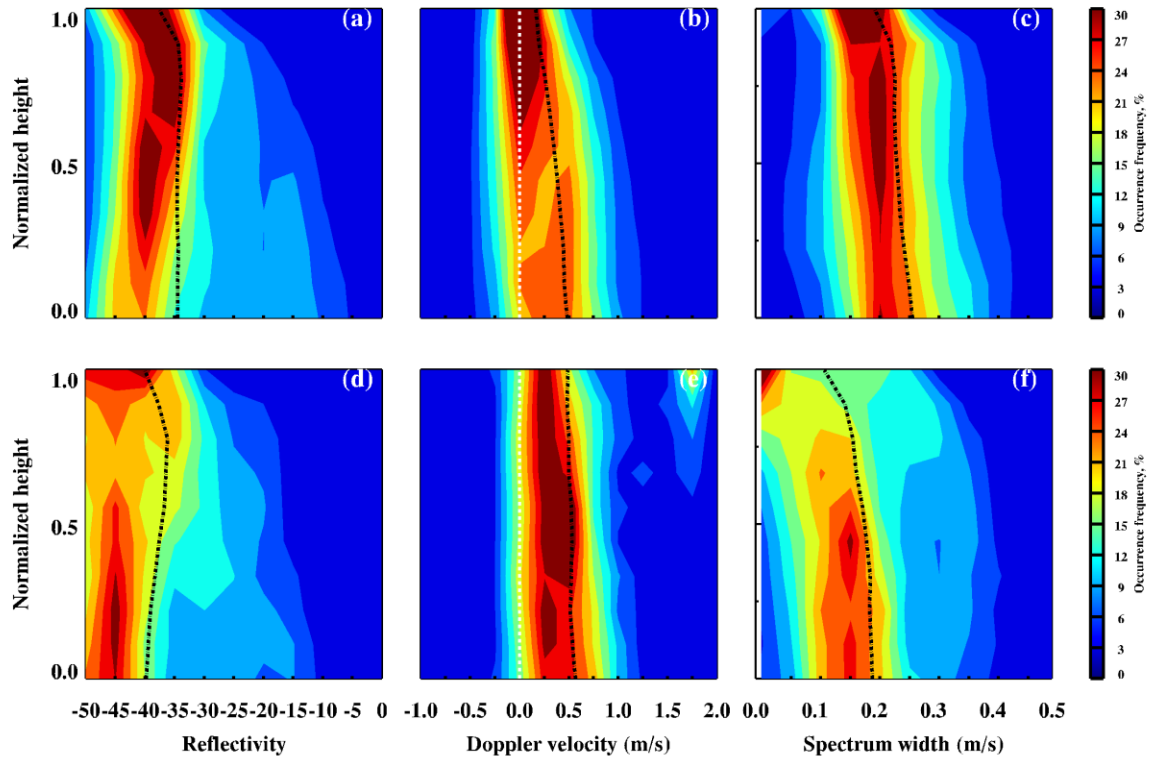
Figure 12. Same as Fig. 11 but only for mixed-phase (a to c, upper panel) and ice (d to f, bottom panel) over the south of 60 °S during MARCUS.